JOSEPHSON JUNCTION CIRCUIT ANALYSIS VIA INTEGRAL MANIFOLDS: PART II

by

M. Odyniec and L. O. Chua

Memorandum No. UCB/ERL M83/12

3 March 1983

JOSEPHSON JUNCTION CIRCUIT ANALYSIS VIA INTEGRAL MANIFOLDS: PART II

by

M. Odyniec and L. O. Chua

Title page

Memorandum No. UCB/ERL M83/12

3 March 1983

ELECTRONICS RESEARCH LABORATORY

College of Engineering
University of California, Berkeley
94720

JOSEPHSON JUNCTION CIRCUIT ANALYSIS VIA INTEGRAL MANIFOLDS: PART II

by

M. Odyniec and L. O. Chua

Memorandum No. UCB/ERL M83/12

3 March 1983

ELECTRONICS RESEARCH LABORATORY

College of Engineering
University of California, Berkeley
94720

JOSEPHSON JUNCTION CIRCUIT ANALYSIS VIA INTEGRAL MANIFOLDS: PART II[†]

M. Odyniec[††] and L.O. Chua[†††]

Abstract

This paper is a sequel to an earlier paper under the same title. Here we use a more realistic model of the Josephson-junction and present a rigorous analysis of its nonlinear dynamics under various ranges of model parameters. In particular, we prove that the qualitative properties of our model and of the simplified one are similar. This rigorous proof thereby justifies the choice of simpler Josephson-junction model, which was chosen in the past mainly for tractability.

The peculiar constant voltage-step phenomenon widely represented in the literature is carefully analyzed further in this paper. For the first time, we can give a fairly complete explanation of the mechanism leading to this exotic phenomenon. In particular, the variations in the length of the constant voltage steps which have baffled many researchers in the past can now be given a rational explanation. A careful analysis of the mechanisms which give rise to chaotic dynamics in the Josephson junction circuit is also presented.

[†]Research supported in part by the Joint Services Electronics Program contract F49620-79-C-0178.

[††]M. Odyniec is on leave from the Institute of Electronics Fundamentals, Technical University of Warsaw, 00-661 Warsaw, Poland.

[†††]L.O. Chua is with the Department of Electrical Engineering and Computer Sciences and the Electronics Research Laboratory, University of California, Berkeley, California 94720

1. Introduction

This paper is a sequel to a recent paper on nonlinear dynamics of the Josephson junction circuit equation [1]

$$C\ddot{\phi} + G\dot{\phi} + \sin(k\phi) = i_s(t) \tag{1}$$

This equation is based on a widely used Josephson junction circuit model consisting of a linear capacitor C, a linear conductance G and a nonlinear inductor described by $i = \sin(k\phi)$. Although this model is widely used in practice and has so far provided answers which agree, at least qualitatively, with measurements, it nevertheless contains a number of approximations which have not been justified on either physical or theoretical grounds.

For example, in the original Josephson paper [2] the second and the third term[1] in equation (1) are replaced by:

$$i(\phi,v) = a(v)\sin(k\phi) + (\sigma_1(v) - \sigma_2(v)\cos(k\phi))v \tag{2}$$

Moreover, the third term in (1) (which models the supercurrent) is a periodic rather than sinusoidal function of ϕ [2,3] [2].

Thus we shall use the circuit model consisting of a linear capacitor C connected in parallel with a nonlinear intrinsic two terminal device J as shown in Fig. 1. If we use this more realistic circuit model, then equation (1) becomes:

$$\begin{aligned} \dot{\phi} &= v \\ C\dot{v} &= i_s(t) - i(\phi,v) \end{aligned} \tag{3}$$

Our objective in this paper is to study the nonlinear dynamics of (3). In particular, we will show that under rather general assumptions on the form of $i(\phi,v)$ and forcing function

$$i_s(t) = I + \varepsilon p(\omega t)$$

---

[1] These terms describe the normal (and quasiparticle) currents and supercurrent.

[2] The authors would like to thank Prof. T. Van Duzer for informative discussion concerning the problem.

equation (3) has the same qualitative properties as its simplified version (1). This study therefore provides a rigorous theoretical justification for using the simplified model even though it was originally chosen mainly for mathematical expediency and tractability.

Our approach will consist of two steps:

1. We shall show that, if the forcing term is constant, i.e., $i_s(t) \equiv I$, then equation (3) posesses in the (ϕ,v,t)-space an invariant surface. Stable trajectories on this surface correspond to steady state solutions of (3). Moreover under small-parameter assumptions, this invariant surface is preserved under the periodic excitation $i_s(t) = I + \varepsilon p(\omega t)$.
2. We shall then discuss possible behaviors of trajectories on an invariant surface (which can be shown to be topologically equivalent to a torus). This discussion explains the peculiar step-wise a.c. junction characteristics and the drastic difference between a.c. and d.c. characteristics. Moreover we offer a theoretical justification for the experimentally known phenomenon that "constant steps" on a.c. characteristics are short for "complicated" frequency ratios. To the best of our knowledge the theoretical justification of this phenomenon was never offered before.

We conclude our study with discussion of possible phenomena which may occur when the small-parameter assumptions are not satisfied. Since this part is mostly illustrative in nature, we will choose the simplified version of Josephson circuit, namely, the one described by equation (1).

2. Small Periodic Perturbation

A. Autonomous case: $i_s(t) \equiv I$

In this section we shall formulate various conditions under which the autonomous equation

$$\begin{aligned} \dot{\phi} &= v \\ \dot{v} &= I - i(\phi,v) \end{aligned} \tag{4}$$

possesses an invariant surface. In order to be specific we assume $I \geq 0$, the case $I < 0$ can be dealt with in a similar way. If moreover $i(-\phi,-v) = -i(\phi,v)$, then the case $I < 0$ can be reduced to $I \geq 0$ by the transformation $\phi \to -\phi$, $v \to -v$. Our approach will be based on the following results proved in [4]:

Theorem 1 Assume that $i(\phi,v)$ in (4) is continuous in ϕ and v, monotonically increasing in v, 2π-periodic in ϕ, and such that for any ϕ there exist (possibly equal to $\pm\infty$) $\lim_{v\to+\infty} i(\phi,v) > 0$ and $\lim_{v\to-\infty} i(\phi,v) < 0$[3]. Assume moreover that $i(\phi,v) < I$ for any ϕ and $v = 0$. Under the above assumptions equation (4) possesses a unique and globally stable invariant surface S_0 shown in Fig. 2, and described by:

$$S_0 = \{(\phi,v,t): v = \psi(\phi),\ \phi \in \mathbb{R},\ t \in \mathbb{R}\} \tag{5}$$

where $\psi(\phi)$ is a continuously differentiable[4] positive and 2π-periodic function of ϕ. Moreover for initial conditions chosen on S_0, equation (4) is equivalent to:

$$\dot{\phi} = \psi(\phi) \tag{6}$$

whose solutions are of the form [1]:

$$\phi(t) = \Omega t + q(t) \tag{7}$$

where $\Omega = 2\pi\left[\int_0^{2\pi} \frac{dx}{\psi(x)}\right]^{-1}$ and $q(t)$ is $\frac{2\pi}{\Omega}$-periodic. It can be shown that γ increases with I and $I-\Omega_I$ tends to zero when I increases [1].

Statement 2, If for some ϕ_0, $i(\phi_0,0) = I$ then (4) has a constant solution $\phi(t) \equiv \phi_0$, $v(t) \equiv 0$. Moreover under some additional conditions, which are expressed in [4] in terms of the phase portrait, (4) may also possess an invariant surface (5) with $\psi(\phi)$ continuously differentiable, positive (provided $I > 0$) and 2π-periodic function of ϕ. Similarly, as in Theorem 1, the equation on the surface is of the form (6).

In terms of the "average" current-voltage characteristic the above results say that as long as $I < \sup_{\phi} i(\phi,0)$, there is a steady-state zero-voltage solution (i.e., constant current results in no voltage drop). Moreover, there exists a periodic steady-state voltage $v(t) = \psi[\Omega t + q(t)]$ having an average value[5] equal

[3] The current expression in (2) as found by Josephson satisfies these assumptions.

[4] If $i(\phi,v)$ is of class C^r then $\psi(\phi)$ is also of class C^r.

[5] Since the junction oscillates at extremely high frequencies (GHz range) only the average value can be measured experimentally.

to $\Omega = \Omega_I$. Thus, if $I < \sup_{\phi} i(\phi,0)$ and the hypotheses of Statement 2 are satisfied, then both constant and periodic steady-state solutions exist simultaneously.

Thus the current v.s. average voltage characteristic is double-valued as shown in Fig. 3.

B. Small Periodic Excitation: $i_s(t) = I + \varepsilon p(\omega t)$

Once the existence and stability of the invariant surface S_0 is established, it can be shown [1,7,8] that this surface is preserved under "small" perturbations of the form $\varepsilon p(\omega t)$. More exactly the following

Theorem 3 [7,8] holds. For small ε there exists an invariant surface S_ε of (3) with $i_s(t) = I + \varepsilon p(\omega t)$ where $p(\tau)$ is 2π-periodic in τ, which can be parametrized as follows:

$$S_\varepsilon = \{(\phi,v,t):\ v = \psi(\phi) + h(\omega t,\phi,\varepsilon),\ \phi \in \mathbb{R},\ t \in \mathbb{R}\} \tag{8}$$

where $\psi(\phi)$ is as defined for surface S_0 (5), and $h(\omega t,\phi,\varepsilon)$ is continuously differentiable[6], $\frac{2\pi}{\omega}$-periodic in t, and 2π-periodic in ϕ. Moreover it is bounded by a constant which decreases to zero with ε[7].

When an initial condition is chosen on S_ε then (3) is equivalent to:

$$\dot{\phi} = f(t,\phi) \tag{9}$$

with $f(t,\phi) \triangleq \psi(\phi) + h(\omega t,\phi,\varepsilon)$ being periodic in both t and ϕ. Because of this double periodicity, the surface S_ε can be viewed as a torus, as shown in Fig. 4.

The proof of the theorem is outlined in [1]. A more detailed discussion is given in [8].

C. The Case of Small C

One can also reduce (3) to an equation on the torus in the case of an arbitrary (not necessarily small) periodic excitation provided the parameter C (junction capacitance) is small.

[6] If $i(\phi,v)$ and $p(\omega t)$ are r-times (continuously) differentiable then $h(\omega t,\phi,\varepsilon)$ is (r-2)-times (continuously) differentiable.

[7] Let us observe that if $\varepsilon = 0$ then $h(\omega t,\phi,0) = 0$ and S_ε coincide with S_0 defined by (5).

Theorem 4 [5,7] Assume that:

a) equation $i_s(t) = i(\phi,v)$ has (for all t and ϕ) a locally unique solution $v = \hat{v}(\phi,t)$ which is bounded and continuous together with its second derivatives,

b) there exists $a > 0$ such that for all ϕ,t

$$\frac{\partial}{\partial v} i[\phi,\hat{v}(\phi,t)] \geq a$$

then for sufficiently small C, equation (3) possesses an invariant surface:

$$S_C = \{(\phi,v,t): v = \hat{v}(\phi,t) + g(\phi,t,C),\ \phi \in \mathbb{R},\ t \in \mathbb{R}\} \tag{10}$$

where $g(\phi,t,C)$ is bounded by a constant D_C such that $D_C \to 0$ as $C \to 0$. Moreover, if $\hat{v}(\phi,t)$, $i_s(t)$, $i(\phi,v)$ are r-times continuously differentiable, then $g(\phi,t,C)$ is (r-2)-times continuously differentiable in ϕ and t.

If $i(\phi,v)$ is 2π-periodic in ϕ so are both $\hat{v}(\phi,t)$ and $g(\phi,t,C)$. If $i_s(t)$ is T-periodic in t, so are both $\hat{v}(\phi,t)$ and $g(\phi,t,C)$. Thus the surface S_C can also be viewed as a torus and (3) can be reduced to

$$\dot{\phi} = \hat{v}(\phi,t) + g(\phi,t,C) \tag{11}$$

Let us note that if the hypothesis of theorems 1-4 are satisfied simultaneously (it means, essentially, that C is small, and the forcing term $i_s(t)$ is of the form $i_s(t) = I + \varepsilon p(\omega t)$ where I is large positive and ε is small) then the surfaces S_ε and S_C coincide. However, in general, these surfaces are different (and their existence is guaranteed by different hypotheses). In particular, for some values of I and small ε, there exist surface S_ε and periodic solutions outside it as shown in Fig. 5(a). In the case of small C, the surface S_C and the periodic solutions may exist simultaneously. In this case the periodic solutions must lie on the surface as shown in Fig. 5(b). The immediate consequence of this property is that in the case of small C the voltage-current characteristic shown in Fig. 3 cannot be double-valued.

3. Equations on Torus

In this section we shall study the properties of solutions which follow from the double periodicity of the invariant surfaces S_ε and S_C. In order to be able to treat simultaneously the cases of small ε and small C we assume $i_s(t) = I + \varepsilon p(\omega t)$[9]. Thus both (9) and (11) can be represented as:

$$\dot{\phi} = f(t,\phi;I) \tag{12}$$

where we introduce I as a parameter to stress the fact that the invariant surfaces and the equations on them depend on I. It is known [1,9] that for any solution of (12) there exists a limit:

$$\mu = \lim_{t\to+\infty} \frac{\phi(t)}{t} \tag{13}$$

which does not depend on any particular solution $\phi(t)$ but only on $f(t,\phi;I)$. Moreover, this limit depends continuously on I, and in some intervals μ is a constant function of I. A typical example of $\mu(I)$ is shown in Fig. 6[10]. It can be shown [9] that $\mu(I)$ is a locally constant function of I over some open interval $(I_0 - \Delta, I_0 + \Delta)$ for some I_0 and $\Delta > 0$, only if μ is a rational number. However, for some I_0, μ can be a rational number and yet not a constant in an arbitrarily small neighborhood of I_0.

For the Josephson-junction circuit in Fig. 1, the number (13) is equal[11] to the <u>average</u> voltage across the Josephson-junction and hence Fig. 6 can be interpreted as the current vs. average-voltage characteristics of the device. The stepwise form of this characteristic was observed experimentally. Moreover constant voltage steps were observed to appear at values which are commensurate with some fixed constant. This result is consistent with the property that μ is constant only at some rational values. Note that in the autonomous ($\varepsilon = 0$) case the right hand side of (12) (which is now independent of t) is either positive for all ϕ, or there is ϕ_0 such that $f(\phi_0;I) = 0$. In the latter case $\mu = \lim_t \frac{\phi_0}{t} = 0$[12]. In the former case, $\phi(t) = \Omega t + q(t)$ (as given by (7))

---

[9] Recall that for small C, ε need not necessarily be small in order to obtain a toroidal invariant surface.

[10] Let us note that in the case of both surfaces S_ε and S_C, the function $f(t,\phi;I)$ increases with I.

[11] With respect to the multiplicative constant [1]

[12] Recall that the rotation number is the same for all solutions of (12).

and $\mu = \lim_{t\to\infty} \frac{\phi(t)}{t} = \Omega$. Hence, in the autonomous case, μ is either zero, or increases with I, and is never (as a function of I) constant as shown in Fig. 3.

B. Synchronization Zones

The natural question to ask is for what rational values will μ be a locally constant function of I. The answer can be given in terms of the so called Poincaré mapping [1,9]. Unfortunately, this mapping cannot, in general, be expressed in analytic form.

In this section we shall give some insight into the domains of stability of μ. Our approach will be based on "the method of averaging" [6,7] and our criteria will be expressed in terms of the right hand side of (12). Consider the case when surfaces S_ε and S_C lie above the $v = 0$ plane in the (t,ϕ,v)-space[13]. We show in Appendix A that equations (9) and (11) can be reduced to the form:

$$\dot{\theta} = \Omega_I + \varepsilon g(\omega t,\theta,\varepsilon) \tag{14}$$

Here Ω_I is defined as in equation (7), and θ is related to the original variable ϕ as depicted in Fig. 7. We shall neglect the dependence of g on I.

Let us fix two relatively prime integers M and N and ask for solutions of (14) which are synchronized to the frequency $\frac{M}{N}\omega$. These solutions must have the form $\theta(t) = \frac{M}{N}\omega t + \alpha(t)$ with $\alpha(t)$ $\frac{2\pi N}{\omega}$-periodic. Hence, the rotation number of $\theta(t)$ is equal to $\frac{M}{N}\omega$. Correspondingly, the rotation number of $\phi(t) = \phi(\theta(t))$ is also equal to $\frac{M}{N}\omega$. We show in Appendix A that the essential information concerning the synchronized solutions can be recovered from the scalar algebraic equation:

$$\Delta = \bar{g}(\alpha) \tag{15}$$

where $\Delta \triangleq \varepsilon^{-1}(\frac{M}{N}\omega - \Omega_I)$ and $\bar{g}(\alpha)$ is $2\pi N$-periodic and continuously differentiable in α. More exactly, the following

Theorem 5 [6,7] holds: If (15) possesses a (constant) solution α_0, such that $\frac{d}{d\alpha} g(\alpha_0) < 0$, then for small $\frac{\varepsilon}{\omega}$, (14) possesses a stable solution

[13] The surface S_ε always lies above the $v = 0$ plane. For S_C, this need not be the case, but (provided that ε is small enough) equation (11) will either have a zero rotation number or will be reducible to (14). For more details, see Appendix A.

$$\theta(t) = \frac{M}{N}\omega t + \bar{\alpha}(t) \tag{16}$$

Here $\bar{\alpha}(t)$ is $\frac{2\pi N}{\omega}$ - periodic and close to α_0.

Remark: Since $\bar{g}(\alpha)$ is $2\pi N$-periodic, the existence of the abovementioned constant solution α_0 implies the existence of a family of constant solution $\alpha_K \triangleq \alpha_0 + K\frac{2\pi}{N}$ $K = 1,\ldots,N-1$ as shown in Fig. 8. Hence, (14) possesses a family of solutions where $\bar{\alpha}_K(t)$ is close to α_K for $K = 0,1,\ldots N-1$.

Define:

$$a \triangleq \inf_{\alpha} \bar{g}(\alpha), \quad b \triangleq \sup_{\alpha} \bar{g}(\alpha). \tag{17}$$

Both a and b depend on M and N (for which (15) was obtained) and their difference tends to zero if either M or N tends to infinity (Appendix A). The property that the difference b-a is "small" for large values if M or N is crucial in the following discussion.

The constant solution of (15) clearly exists if $\Delta \in (a,b)$[14]. Let us investigate this condition in terms of ω, Ω_I, ε, M and N. Suppose $\frac{M}{N}$ and ω are fixed, then Ω_I must satisfy $\varepsilon a < \frac{M}{N}\omega - \Omega_I < \varepsilon b$ i.e., $\frac{M}{N}\omega - \varepsilon b < \Omega_I < \frac{M}{N}\omega - \varepsilon a$. This inequality is depicted in Figs. 9(a) and (b) where the necessary conditions for synchronization are satisfied within the shaded region. If we let M and N vary, then Fig. 9 contains many synchronization zones[15]. Observe that since a-b tend to zero as $N \to \infty$, or as $M \to \infty$, we can expect the zones corresponding to $\frac{M}{N}$ with either M or N large to be narrow. In Figs. 10(a) and (b) we show examples of (possible) synchronization zones for $\frac{M}{N} = \frac{1}{2}$, $\frac{M}{N} = \frac{17}{20}$, and $\frac{M}{N} = 1$. Let us note that Figures 9 and 10 are valid only for ε "small enough" (and that "small enough" must be smaller for small ω) i.e., as long as theorem 5 holds.

Now, let us fix $\varepsilon = \varepsilon_0$ (small) and $\omega = \omega_0$ and let Ω_I and M,N vary. When increasing Ω_I we shall pass from one synchronization zone to another in the (Ω_I,ω)-plane and rational rotation numbers will be obtained as shown in Figs. 11(a) and (b). Now, knowing Ω_I as a function of I and combining it with Fig. 11(b), we obtain the stepwise charateristic of μ as shown in Fig. 12, where the longer[16] steps for M and N correspond to small integers. Finally note that if we fix Ω_I in Fig. 10(b) and let ω, ε and M, N vary, we shall

---

[14] if $\Delta = a$ or $\Delta = b$ the solution also exists but then $\frac{d}{d\alpha}\bar{g}(\alpha) = 0$ and Theorem 5 does not hold.

[15] More exactly we should call them "zones of possible synchronization" since if (15) has a constant solution we still need $\frac{d}{d\alpha}\bar{g}(\alpha) < 0$ to guarantee synchronization.

[16] Figs. 9 to 11 show only zones where synchronization may appear. Thus we know that steps obtained for large M and N must be small and those obtained for small M and N may be large.

obtain the well-known [20] relation shown in Fig. 13

$$\frac{N}{M}(\Omega_I + \varepsilon a) < \omega < \frac{N}{M}(\Omega_I + \varepsilon b).$$

This implies that the smaller the perturbation is, the closer must $\frac{M}{N}\omega$ approach the natural frequency Ω_I in order to obtain synchronization. Note also for ε "very small" all the steps are very narrow and the rotation number characteristics approaches that of Ω_I as shown in Fig. 14.

4. Strange Phenomena

In this section we shall study various phenomena which can appear when the small-parameter assumptions are not satisfied. It was observed experimentally that for some parameter values, the Josephson-junction circuit in Fig. 1 behaves in an erratic manner [15-17,19]. Our aim in this section is to give some geometric insights concerning this "strange" behavior and to predict the parameter values for which it can appear.

Consider the nonautonomous Josephson junction circuit equation[17]

$$\begin{aligned} \dot{\phi} &= v \\ C\dot{v} &= I - Gv - \sin(k\phi) + \varepsilon p(\omega t) \end{aligned} \tag{17}$$

where $p(\tau)$ is 2π-periodic in τ and $\sup_{\tau}|p(\tau)| = 1$. If $\varepsilon = 0$, then there exists a critical value I_0 such that for $I > I_0$ the resulting autonomous system possesses an invariant[18] surface as shown in Fig. 15(a), but for $I < I_0$ it does not [1], as shown in Fig. 15(c). The "invariant surface" in Fig. 15(b) is not structurally stable in the sense that a small change in the value of the parameter I from I_0 changes the topological behavior in a drastic way; namely from Fig. 15(a) to Fig. 15(c). Now let $I = I_0$, $\varepsilon \neq 0$ and let us take intersections at time $t = 0, \frac{2\pi}{\omega}, 2(\frac{2\pi}{\omega}),..,.$ Since $p(\omega t)$ in (17) is $\frac{2\pi}{\omega}$-periodic in t, the intersection at each time $t_K = K(\frac{2\pi}{\omega})$ will be the same. Moreover, the invariant surface S can bifurcate into three different ways as shown in

---

[17] To be specific, we consider the simplest form of the Josephson junction equation. Our discussion, however, will be couched in terms of phase portraits and therefore remains valid for more general equations.

[18] All trajectories originating from points on the surface S must remain on the surface S.

Fig. 16[19][11,12,13]. One possibility is that the surfaces do not intersect as shown in Figs. 16(a) and (b), (and in the (t,ϕ,v)-space, in Figs. 17(a) and (b)). When invariant surfaces do intersect each other the situation is drastically different. Observe first that if there is one intersention, then there must be infinitely many of them[20] as shown in Fig. 18. In view of the infinite number of intersections, we can represent in the (t,ϕ,v)-space only a small part of the intersecting surfaces in Fig. 19.

Since the right-hand side of (17) is periodic in ϕ, the global phase portrait will also be periodic in ϕ. If one identifies now ϕ and $\phi + K(2\pi)$, and considers behavior of points in the domain D_0 as shown in Fig. 20, one obtains extremely complicated behaviors among intertwining trajectories. In Fig. 20, D_K, $K = 0,\pm1,\pm2,\ldots$ denotes the domains where points from some domain D_0 will go after K (forward or backward) periods. This complicated behavior was first described rigorously by Smale [10]. In particular Smale shows that the portrait in Fig. 20 includes periodic solutions of any period and that trajectories behave in a "chaotic" way in a sense which can be specified precisely [11,12]. Such a chaotic behavior was also observed in numerical [15,16] and analog [17] experiments. It remains to be shown that indeed in the considered range of parameters the invariant surfaces do intersect. In Appendix B we review the method by Melnikov [12,13,14] and use it to prove that in the case of small G and small ε the surfaces do intersect. A different approach was applied by Belykh and Belyustina [18,19]. They considered together with (17) two autonomous equations obtained from (17) by letting $p(\omega t) \equiv 1$ and $p(\omega t) \equiv -1$. Study of these (autonomous) equations allowed them to find domains in which invariant surfaces of (17) lie. In the same way they obtained parameters for which these surfaces intersect, thereby giving rise to chaotic behaviors.

Both Melnikov's and Belykh-Belyustina's methods predict chaotic behaviors for I close to the critical[21] value, and for ε which is "not too large." These results are consistent with computer data reported in [15,17].

[19] Fig. 16 shows the intersection of surface S with a constant time plane at $t = k(\frac{2\pi}{\omega})$. There are more bifurcation possibilities than those shown in Fig. 16. However, the portraits shown, are the only ones which are structurally stable, i.e., those which persist under small perturbation.

[20] Each point of intersection belongs to both invariant surfaces and so does the trajectory originating from it. Now this trajectory tends to $\bar{\phi}$ as $t \to -\infty$ and to $\bar{\phi}+2\pi$ as $t \to +\infty$. The sequence of points $(v(K\frac{2\pi}{\omega}), \phi(K\frac{2\pi}{\omega}))$, $K = 0,\pm1,\pm2\ldots$ lies on both surfaces and therefore constitutes infinitely many points of intersections.

[21] i.e., corresponding to the "saddle connection" of the autonomous system as shown in Fig. 15(b).

Note that as shown in Sections 2, 3 and in [1] if one chooses I larger than the critical value I_0 first, and then chooses ε "small enough" then the existence of the invariant surface S_ε is guaranteed and no chaos occurs. Note also that for small C, as guaranteed by Theorem 4, no chaos occurs.

The chaotic behavior was observed also by Huberman et al [16] for $I = 0$ and ε "large" as shown in Fig. 21. Because of the large periodic perturbation it may be possible for invariant surfaces to intersect even for I far from the critical value. However no proof of this phenomenon presently exists.

APPENDIX A

A. Equation on the torus and synchronization zones: small ε case

A1. Change of variables

Consider equation (7):

$$\dot{\phi} = \psi(\phi)+h(\omega t,\phi,\varepsilon) \tag{A1}$$

It can be shown that there exists a positive constant d such that $\psi(\phi) \geq d$ for all ϕ [4]. Moreover, $h(\omega t,\phi,\varepsilon)$ is differentiable in ε, and since $h(\omega t,\phi,0) = 0$ it can be represented as [7,8]

$$h(\omega t,\phi,\varepsilon) = \varepsilon h_1(\omega t,\phi,\varepsilon) \tag{A2}$$

Consider now (11) (i.e., equation on the S_C-surface)

$$\dot{\phi} = \hat{v}(\phi,t) + g(\phi,t,C) \tag{A3}$$

where $\hat{v}(\phi,t)$ is obtained from:

$$I + \varepsilon p(\omega t) = i(\phi,\hat{v}(\phi,t)) \ .$$

Since $i_s(t)$ is of the form $I + \varepsilon p(\omega t)$ the functions $\hat{v}$ and g can be represented[22], respectively, as follow:

$$\begin{aligned} \hat{v}(\phi,t) &= \hat{v}_1(\phi) + \varepsilon v_2(\phi,t,\varepsilon) \\ g(\phi,t,C) &= g_1(\phi,C) + g_2(\phi,t,\varepsilon,C) \end{aligned} \tag{A4}$$

Thus, (A3) can be reduced to the form (A1) with $\psi(\phi) \triangleq v_1(\phi) + g_1(\phi,C)$ where $g_1(\phi,C)$ is "small" for small C. Now if there exists ϕ_0 such that $v_1(\phi_0) = 0$

[22] The case for $\hat{v}$ follows from the hypotheses of theorem 4 and the implicit function theorem. In the case of g the property follows from the construction of the Surface S_C.

and $\frac{dv_1(\phi_0)}{d\phi} \neq 0$[23] then the rotation number of (11) is zero (provided C and ε are small enough). Since we are interested in nonzero rotation numbers we shall assume that $v_1(\phi) > 0$; i.e., equation (11) is reducible (for small ε and C) to (A1) with the condition $\psi(\phi) \geq d \geq 0$ for all ϕ. Let us introduce now the new variable:

$$\theta \triangleq \theta(\phi) = \Omega \int_0^{\phi} \frac{dx}{\psi(x)} \tag{A5}$$

where $\Omega \triangleq 2\pi \left[\int_0^{2\pi} \frac{dx}{\psi(x)}\right]^{-1}$

Observe that $\frac{d\theta}{d\phi} = \Omega/\psi(\phi) > 0$. Thus $\theta(\phi)$ is monotonically increasing (and, as such, invertible) and $\theta(\phi+2\pi) = \theta(\phi)+2\pi$ for all ϕ. Clearly,

$$\theta(\phi) = \phi+\eta(\phi) \tag{A6}$$

where $\eta(\phi)$ is 2π-periodic. The same relationship holds for the inverse function

$$\phi(\theta) = \theta+\zeta(\theta) \tag{A7}$$

where $\zeta(\theta)$ is 2π-periodic. The θ vs. ϕ relationship is depicted in Fig. 7. Observe also that:

$$\frac{d\theta}{dt} = \frac{d\theta}{d\phi} \cdot \frac{d\phi}{dt} = (\Omega/\psi(\phi))\frac{d\phi}{dt}$$

Hence, (A1) can be reduced to the form

$$\dot{\theta} = \Omega + \varepsilon g(\omega t,\theta,\varepsilon) \tag{A8}$$

where $g(\omega t,\theta,\varepsilon) \triangleq \varepsilon\Omega h_1(\omega t,\theta(\phi),\varepsilon)/\psi(\theta) = \Omega h(\omega t,\phi(\theta),\varepsilon)/\psi(\theta)$.

It is an immediate consequence of (A7) that <u>the rotation number of (A8) is the same as that of (A1)</u>. Indeed, let the rotation number of (A8) be μ, then $\theta(t) = \mu t + \gamma(t)$ with $\gamma(t)$ bounded. Now

$$\lim_{t\to\infty} \frac{\phi(t)}{t} = \lim_{t\to\infty} \frac{\phi(\theta(t))}{\theta(t)} \cdot \frac{\theta(t)}{t} = \lim_{\theta\to\infty} \frac{\phi(\theta)}{\theta} \cdot \mu$$

and because of (A7), $\lim_{\theta\to\infty} \frac{\phi(\theta)}{\theta} = 1$. □

[23] This would be the case if $\frac{\partial}{\partial\phi} i(\phi_0,0) \neq 0$ where $i(\phi,v)$ is given in (3)

A2. Synchronization zones

The function $g(\omega t,\theta,\varepsilon)$ which appears in (A8) is 2π-periodic in θ and $\frac{2\pi}{\omega}$-periodic in t. Let us expand it into a Fourier series:

$$g(\omega t,\theta,\varepsilon) = \sum g_{m,n} e^{jm\omega t} e^{jn\theta} \tag{A9}$$

where $g_{m,n} = \int_0^{2\pi}\int_0^{2\pi} g(\tau,\theta,0)e^{-jm\tau}e^{-jn\theta}d\tau d\theta$. Let us fix the integers M and N, and define

$$\Delta = \varepsilon^{-1}[\tfrac{M}{N}\omega-\Omega] \tag{A10}$$

We shall assume that Δ remains bounded for small ε; i.e., for small ε the frequencies $\frac{M}{N}\omega$ and Ω must remain close to each other. Define also $\alpha(t) \triangleq \theta(t) - \frac{M}{N}\omega t$. Under this notation (A8) takes the form:

$$\dot{\alpha} = \varepsilon[-\Delta + \sum_{m,n} g_{m,n} e^{jm\omega t} e^{jn(\frac{M}{N}\omega t+\alpha)}] \tag{A11}$$

and, when averaged in time, it reduces to

$$\dot{\alpha} = \varepsilon[-\Delta+\bar{g}(\alpha)] \tag{A12}$$

where $\bar{g}(\alpha) = \sum_{\ell} g_{\ell M,-\ell N} e^{-j\ell N\alpha}$ is $2\pi N$-periodic in α. The following

Theorem holds [6,7,8]: Assume (A12) has a constant solution α_0 such that $\frac{d}{d\alpha}\bar{g}(\alpha_0) < -\delta$, for some positive constant δ (independent of ε). Then for $\frac{\varepsilon}{\omega}$ "sufficiently small" (A11) has a stable $\frac{2\pi N}{\omega}$-periodic solution $\alpha(t)$ which is close to α_0.

Clearly, the necessary condition for the existence of a constant solution for (A12) is

$$\inf_{\alpha} \bar{g}(\alpha) \triangleq a < \Delta < b = \sup_{\alpha} \bar{g}(\alpha) \tag{A13}$$

Moreover:

$$\sup_{\alpha} \bar{g}(\alpha) - \inf_{\alpha} \bar{g}(\alpha) < B_{M,N} = 2 \sum_{\ell\neq 0} |g_{\ell M,-\ell N}|$$

Observe that $B_{M,N} \to 0$ as $M \to \infty$ or as $N \to \infty$. Indeed, if $\bar{g}(\alpha)$ is r times continuously differentiable, then $n^r m^r g_{n,m} \to 0$ as $n \to \infty$ or as $m \to \infty$.

It follows that for M or N "large enough" the entire sum $B_{M,N}$ will be small. Thus, the zones of possible synchronization in the (ω,ε)-plane will appear as shown in Fig. A1. Note that since ε must be small with respect to ω, the zones for small ω are lower.

APPENDIX B

B Melnikov's Method[24] [12,13,14]

B1. General Theory

Consider

$$\dot{x} = f(x) + \varepsilon g(t,x) \tag{B1}$$

where x,f,g are continuously differentiable vector-valued functions, $g(t+T,x) = g(t,x)$, and ε is a small parameter.

Suppose that the unperturbed equation

$$\dot{x} = f(x) \tag{B2}$$

possesses two saddle points and a saddle connection Γ_0 as shown in Fig. B1(a). The points x_{01}, x_{02} may coincide and give rise to a homoclinic orbit as shown in Fig. B1(b). We shall give conditions under which the perturbed equation (B1) will possess a heteroclinic structure or a homoclinic structure as shown in Figs. B1(c) and (d) respectively. The following

Lemma B1 [11,12] holds: If ε is small, then (B1) possesses in a neighborhood of x_{01} and x_{02} unique periodic solutions $x_1(t)$ and $x_2(t)$. Moreover each of these solutions has a stable and an unstable manifold. □

Let x_1, x_2 represent the abovementioned periodic solutions, and let $W^u(x_1)$ and $W^s(x_2)$ denote respectively the unstable and stable manifolds in a Poincaré section as shown in Fig. B2.

Let us denote the time for which the Poincaré section was taken by t_0. Let $q_0(t,t_0) = q_0(t-t_0)$ denote the solution on $\Gamma_0 x(-\infty,+\infty)$, and let $q_\varepsilon^u(t,t_0)$ denote the solutions on $W^u(x_1)x(-\infty,+\infty)$ and $W^s(x_2)x(-\infty,+\infty)$, respectively

Lemma B2 [12,13] Trajectories on $W^u(x_1)x(-\infty,+\infty)$ and $W^s(x_2)x(-\infty,+\infty)$ can be expressed as follows:

[24]Discussions on this subject with R.D. Rand, Y.S. Tang, and T.S. Parker are gratefully acknowledged.

$$q_\varepsilon^s(t,t_0) = q_0(t-t_0) + \varepsilon q_1^s(t,t_0) + O(\varepsilon^2),\ t \in [t_0,+\infty)$$
$$q^u(t,t_0) = q_0(t-t_0) + \varepsilon q_1^u(t,t_0) + O(\varepsilon^2),\ t \in (-\infty,t_0] \tag{B3}$$

where $q^{s,u}(t,t_0)$ are bounded. □

The functions $q_\varepsilon^{s,u}(t,t_0)$ are uniquely defined by orthogonal projection of $q_0(t_0-t_0) = q_0(0)$ on $W^u(x_1)$ and $W^s(x_2)$ as shown in Fig. B2. Define now the <u>separation</u> between manifolds $W^u(x_1)$ and $W^s(x_2)$ by

$$d(t_0) \triangleq \frac{f[q_0(0)] \wedge [q^u(t_0,t_0) - q^s(t_0,t_0)]}{|f[q_0(0)]|} \tag{B4}$$

where

$$a \wedge b = \begin{bmatrix} a_1 \\ a_2 \end{bmatrix} \wedge \begin{bmatrix} b_1 \\ b_2 \end{bmatrix} \triangleq a_1b_2 - a_2b_1 = |a| \cdot |b| \sin\measuredangle(a,b)$$

from Lemma B.2 $d(t_0) = \varepsilon \dfrac{f[q_0(0)] \wedge [q_1^u - q_1^s]}{|f[q_0(0)]|} + O(\varepsilon^2)$

where $q_1^{u,s} = q_1^{u,s}(t_0,t_0)$.

Introduce

$$\Delta^u(t,t_0) := f[q_0(t-t_0)] \wedge q_1^u(t,t_0)$$
$$\Delta^s(t,t_0) := f[q_0(t-t_0)] \wedge q_1^s(t,t_0) \tag{B5}$$
and $$\Delta(t,t_0) := \Delta^u(t,t_0) - \Delta^s(t,t_0)$$

Using this notation, we have

$$d(t_0) = \frac{\varepsilon}{|f(q_0(0))|} \cdot \Delta(t_0,t_0) + O(\varepsilon^2) \tag{B6}$$

Observe that if $\Delta(t_0,t_0)$ changes its sign (when t_0 is changed) then $W^u(x_1)$ and $W^s(x_2)$ intersect each other. In particular, if $\frac{d}{dt_0}\Delta(\bar{t}_0,\bar{t}_0) \neq 0$ and $\Delta(\bar{t}_0,\bar{t}_0) = 0$ then the intersection is transversal[25]. On the other hand, if there exists

[25]Intersection is said to be transversal if it persists under small perturbation.

$\delta > 0$ such that $|\Delta(t_0,t_0)| > \delta$ for all t_0, then for small ε, $W^u(x_1)$ and $W^u(x_2)$ do not intersect each other.

Lemma B.3 [13]

If $\exp[\pm \int_0^{\pm\infty} \operatorname{div} f[q_0(\tau)]d\tau]$ is bounded then

$$\Delta(t_0,t_0) = \int_{-\infty}^{+\infty} f[q_0(t-t_0)] \wedge g[t,q_0(t-t_0)] \cdot \exp\{-\int_0^{t-t_0} \operatorname{div} f[q_0(\tau)]d\tau\}dt \tag{B7}$$

In particular, if $\operatorname{div} f[q_0(\tau)] = 0$
then

$$\Delta(t_0,t_0) = \int_{-\infty}^{+\infty} f[q_0(\tau)] \wedge g[\tau + t_0, q_0(\tau)]d\tau$$

Proof: Consider $\Delta^u(t,t_0)$ as defined in (B5)

$$\frac{d}{dt}\Delta^u(t,t_0) = \frac{d}{dt} f[q_0(t-t_0)] \wedge q_1^u(t,t_0)$$

$$= f'[q_0(t-t_0)]\, \dot{q}_0(t-t_0) \wedge q_1^u(t,t_0) + f(q_0(t-t_0)] \wedge \dot{q}_1^u(t,t_0)$$

Let us recall that

$$\dot{q}_0 = f(q_0), \text{ and } \dot{q}_\varepsilon^u = f(q_\varepsilon^u) + \varepsilon g(t,q_\varepsilon^u).$$

Since: $q_\varepsilon^u = q_0 + \varepsilon q_1^u + O(\varepsilon^2)$

we have: $\dot{q}_0 + \varepsilon\dot{q}_1 + O(\varepsilon^2) = f(q_0) + f'(q_0)\, \varepsilon q_1^u + \varepsilon g(t,q_0) + O(\varepsilon^2)$

and $\dot{q}_1 = f(q_0)\, q_1^u + g(t,q_0)$

Thus:

$$\frac{d}{dt}\Delta^u(t,t_0) = f'[q_0]\cdot f(q_0) \wedge q_1^u + f[q_0] \wedge f'(q_0) q_1^u + f[q_0] \wedge g(t,q_0)$$

$$= \operatorname{div} f[q_0(t-t_0)]\cdot \Delta^u(t,t_0) + f[q_0(t-t_0)] \wedge g[t,q_0(t-t_0)].$$

To prove the last equality take $f'(q_0) =: \begin{bmatrix} f_{11} & f_{12} \\ f_{21} & f_{22} \end{bmatrix}$, $f(q_0) = \begin{bmatrix} f_1 \\ f_2 \end{bmatrix}$, $q = \begin{bmatrix} q_1 \\ q_2 \end{bmatrix}$

$$\begin{bmatrix} f_{11} \cdot f_1 + f_{12} \cdot f_2 \\ f_{21} \cdot f_1 + f_{22} \cdot f_2 \end{bmatrix} \wedge \begin{bmatrix} q_1 \\ q_2 \end{bmatrix} + \begin{bmatrix} f_1 \\ f_2 \end{bmatrix} \wedge \begin{bmatrix} f_{11} \cdot q_1 + f_{12} \cdot q_2 \\ f_{21} \cdot q_1 + f_{22} \cdot q_2 \end{bmatrix} =$$

$$f_{11}f_1q_2 + f_{12}f_2q_2 - f_{21}f_1q_1 - f_{22}f_2q_1 + f_1f_{21}q_1 + f_1f_{22}q_2 - f_2f_{12}q_2 =$$

$$(f_{11} + f_{22})(f_1q_2 - f_2q_1) = \operatorname{tr} f'(q_0) \cdot (f(q_0) \wedge q_1^u) = \operatorname{div} f \cdot \Delta^u$$

In a similar way, one proves that

$$\frac{d}{dt} \Delta^s(t,t_0) = \operatorname{div} f[q_0(t-t_0)]\, \Delta^s(t,t_0) + f[q_0(t-t_0)] \wedge g(t,q_0(t-t_0))$$

i.e., both Δ^u and Δ^s satisfy an equation of the form

$$\dot{\xi} = a(t)\xi + b(t)$$

The solution:

$$\xi(t) = e^{\int_{t_0}^{t} a(\tau)d\tau} \cdot \xi(t_0) + \int_{t_0}^{t} b(\tau) e^{\int_{\tau}^{t} a(s)ds} d\tau$$

is equivalent to:

$$\xi(t_0) = \xi(t) e^{-\int_{t_0}^{t} a(\tau)d\tau} - \int_{t_0}^{t} b(\tau) e^{\int_{\tau}^{t_0} a(s)ds} d\tau \qquad \text{(B8)}$$

now

(a) if $e^{\int_{t_0}^{-\infty} a(\tau)d\tau}$ is bounded and $\xi(t) \underset{t \to -\infty}{\to} 0$ then

$$\xi(t_0) = -\int_{t_0}^{-\infty} b(\tau) e^{\int_{\tau}^{t_0} a(s)ds} d\tau$$

(b) if $e^{\int_{t_0}^{+\infty} a(\tau)d\tau}$ is bounded and $\xi(t)_{t\to+\infty}$ 0 then

$$\xi(t_0) = -\int_{t_0}^{+\infty} b(\tau)e^{\int_{\tau}^{t_0} a(s)ds}\,d\tau$$

Recall that $f[q_0(t-t_0)] \underset{t\to\pm\infty}{\to} 0$ and by Lemma B.2 $q_1^{s,u}(t,t_0)$ is bounded.

Hence, $\Delta^u(t,t_0) \underset{t\to-\infty}{\to} 0$, $\Delta^s(t,t_0) \underset{t\to+\infty}{\to} 0$.

By assumption, $\exp[\pm\int_0^{\pm\infty} \text{div } f]$ is bounded and by properties (a) and (b) above we have:

$$\Delta^u(t_0,t_0) = -\int_{t_0}^{-\infty} f[q_0(\tau-t_0)] \wedge g[\tau,q_0(\tau-t_0)]\cdot\exp\{\int_{\tau}^{t_0} \text{div } f[q_0(\tau-t_0)]ds\}d\tau$$

$$\Delta^s(t_0,t_0) = -\int_{t_0}^{-\infty} f[q_0(\tau-t_0)]\ \ g[\tau,q_0(\tau-t_0)]\ \exp\{\int_{t}^{t_0} \text{div } f[q_0(s-t_0)]ds\}d\tau$$

Hence,

$$\begin{aligned}\Delta(t_0,t_0) &\triangleq \Delta^u(t_0,t_0) - \Delta^s(t_0,t_0)\\ &= \int_{-\infty}^{+\infty} f[q_0(\tau-t_0)]\exp\{\int_{\tau-t_0}^{0} \text{div } f[q_0(\sigma)]d\sigma\}d\tau\\ &= \int_{-\infty}^{+\infty} f[q_0(t)]\wedge g[t+t_0,q_0(t)]e^{-\int_0^t \text{div } f[q_0(\sigma)]d\sigma}\,dt \qquad \square\end{aligned}$$

B2. Example. Pendulum with Weak Damping and Forcing[26]

Consider $\dot{x} = y$

$$\dot{y} = -\sin x + \varepsilon a y + \varepsilon b \sin\omega t \qquad (B9)$$

[26]The system considered is equivalent to the Josephson-junction circuit described by (4.1) with $p(\omega t) = b\sin\omega t$, $I = 0$, $G = \varepsilon a$, $k = 1$, and $C = 1$.

This equation is of the form (B1) with:

$$x = \begin{bmatrix} x \\ y \end{bmatrix}, \quad f(x) = \begin{bmatrix} y \\ \sin x \end{bmatrix}, \quad g(t,x) = \begin{bmatrix} 0 \\ -ay + b \sin \omega t \end{bmatrix}$$

$$f(x) \wedge g(t,x) = -ay^2 + by \sin \omega t.$$

Hence,

$$\Delta(t_0,t_0) = \int_{-\infty}^{+\infty} (-ay^2(t) + by_0(t)\sin\omega(t+t_0))dt$$

where $y_0(t-t_0)$ denotes the solution on Γ_0 as shown in Fig. B.3. (obtained for $\varepsilon = 0$). Let us choose t_0 and $y_0(0)$ so that $y_0(\tau)$ is an even function.

With $y_0(\tau)$ chosen as above, $\Delta(t_0,t_0)$ takes the form:

$$\Delta(t_0,t_0) = -aA + bB \sin \omega t_0 \tag{B10}$$

where

$$A := \int_{-\infty}^{+\infty} y_0^2(t)dt$$

$$B := \int_{-\infty}^{+\infty} y_0(t)\cos\omega t dt$$

It follows from (B10) that

(a) If $\left|\frac{a}{b}\right| > \left|\frac{B}{A}\right|$, then $\Delta(t_0,t_0) \neq 0$ for $t_0 \in [0,\frac{2\pi}{\omega}]$

and for ε small enough, W^S and W^u never intersect each other as shown in Fig. B4. In particular, these manifolds do not intersect when periodic forcing is absent (i.e., $b = 0$, $a > 0$)

(b) If $\left|\frac{a}{b}\right| < \left|\frac{B}{A}\right|$, then $\Delta(t_0,t_0)$ changes its sign at $\bar{t}_0$ defined by $aA = bB\sin\omega\bar{t}_0$

Note that $\frac{d}{dt_0}\Delta(\bar{t}_0,\bar{t}_0) = +\omega bB\cos\omega\bar{t}_0 = \omega\sqrt{(bB)^2 - (aA)^2} \neq 0$

So for ε small enough, the manifolds intersect transversally. Regions of the (a,b) parameter plane where chaos exists are shaded in the Fig. B5.

Footnotes:

1. These terms describe the normal (and quasiparticle) currents and supercurrent.
2. The authors would like to thank Prof. T. Van Duzer for informative discussion concerning the problem.
3. The current expression in (2) as found by Josephson satisfies these assumptions.
4. If $i(\phi,v)$ is of class C^r then $\psi(\phi)$ is also of class C^r.
5. Since the junction oscillates at extremely high frequencies (GHz range) only the average value can be measured experimentally.
6. If $i(\phi,v)$ and $p(\omega t)$ are r-times (continuously) differentiable then $h(\omega t,\phi,\varepsilon)$ is (r-2)-times (continuously) differentiable.
7. Let us observe that if $\varepsilon = 0$ then $h(\omega t,\psi,0) = 0$ and S_ε coincides with S_0 defined by (5).
9. Recall that for small C, ε need not necessarily be small in order to obtain a toroidal invariant surface.
10. Let us note that in the case of both surfaces S_ε and S_C, the functions $f(t,\phi;I)$ increases with I.
11. With respect to the multiplicative constant [1].
12. Recall that the rotation number is the same for all solutions of (12).
13. The surface S_ε always lie above the $v = 0$ plane. For S_C, this need not be the case, but (provided that ε is small enough) equation (11) will either have a zero rotation number or will be reducible to (14). For more details, see Appendix A.
14. If $\Delta = a$ or $\Delta = b$ the solution also exists but then $\frac{d}{d\alpha}\bar{g}(\alpha_0) = 0$ and Theorem 5 does not hold.
15. More exactly we should call them "zones of possible synchronization" since if (15) has a constant solution we still need $\frac{d}{d\alpha}\bar{g}(\alpha_0) < 0$ to guarantee synchronization.
16. Figs. 9 to 11 show only zones where synchronization <u>may</u> appear. Thus we know that steps obtained for large M and N <u>must be small</u> and those obtained for small M and N <u>may be</u> large.

17. To be specific, we consider the simplest form of the Josephson junction equation. Our discussion, however, will be couched in terms of phase portraits and therefore remains valid for more general equations.
18. All trajectories originating from points on the surface S must remain on the surface S.
19. Fig. 16 shows the intersection of surface S with a constant time plane at $t = k(\frac{2\pi}{\omega})$. There are more bifurcation possibilities than those shown in Fig. 16. However, the portraits shown are the only ones which are structurally stable; i.e., those which persist under small perturbation.
20. Each point of intersection belongs to both invariant surfaces and so does the trajectory originating from it. Now this trajectory tends to $\bar{\phi}$ as $t \to -\infty$ and to $\varphi + 2\pi$ as $t \to +\infty$. The sequence of points $(v(k\frac{2\pi}{\omega}))$, $k = 0, \pm 1, \pm 2, \ldots$ lies on both surfaces and therefore constitutes infinitely many points of intersections.
21. i.e., corresponding to the "saddle connection" of the autonomous system as shown in Fig. 15(b).
22. The case for $\hat{v}$ follows from the hypotheses of theorem 4 and the implicit function theorem. In the case of g the property follows from the construction of the surface S_c.
23. This would be the case if $\frac{\partial}{\partial \phi}\, i(\phi_0, 0) \neq 0$ where $i(\phi, v)$ is given in (3).
24. Discussions on this subject with R.D. Rand, Y.S. Tang, and T.S. Parker are gratefully acknowledged.
25. Intersection is said to be transversal if it persists under small perturbation.
26. The system considered is equivalent to the Josephson-junction circuit described by (4.1) with $p(\omega t) = b \sin \omega t$, $I = 0$, $G = \varepsilon a$, $k = 1$, and $C = 1$.

Figure Captions

Fig. 1. A Josephson-junction circuit model.

Fig. 2. The surface S_0 in the (t,ϕ,v)-space.

Fig. 3. The average-voltage vs. d.c.-current characteristic. Note the critical value for I_0 such that $I_0 \leq I \leq I_1 = \sup_{\phi} i(\phi,0)$ the characteristic is double-valued.

Fig. 4. The invariant surface S_ε can be viewed as a "cylinder" or a "torus."

Fig. 5. The surfaces S_ε and S_C may coexist with periodic solutions. (a) In case of small ε the periodic solutions must lie outside the surface S_ε (b) In case of small C the periodic solutions lie on the surface S_C.

Fig. 6. The rotation number as a function of I is a continuous and nondecreasing function.

Fig. 7. The old variable ϕ versus the new one θ.

Fig. 8. The function $\bar{g}(\alpha)$ is $\frac{2\pi}{N}$ -periodic. Note that we are considering only these solutions α_K for which $\frac{d}{d\alpha}\bar{g}(\alpha_K) < 0$.

Fig. 9. The possible synchronization zone obtained for $\frac{M}{N}$ frequency ratio.
(a) The forcing frequency ω is fixed
(b) The synchronization zone in the $(\omega,\Omega_I,\varepsilon)$-space. Observe, that if the forcing frequency ω is "small" then the forcing amplitude ε must also be "small."

Fig. 10. Example of possible synchronization zones obtained for different frequency ratios (a) for ω fixed in the (Ω_I,ε)-plane, (b) in the $(\omega,\Omega_I,\varepsilon)$-space.

Fig. 11. (a) The synchronization zones from the Fig. 10(b) shown for fixed ε
(b) If $\omega = \omega_0$ is fixed then the rotation number changes with Ω_I. Note that it remains constant within each synchronization zone.

Fig. 12. Graphical method of obtaining μ as a function of I if the dependence of μ on Ω_I is known.

Fig. 13. Possible synchronization zones for Ω_I fixed.

Fig. 14. The rotation number versus d.c.-current in case when a.c.-current amplitude is small.

Fig. 15. The invariant surface and the constant solutions for d.c. forcing $I < I_1$.
(a) $I_0 < I < I_1$, the constant solutions lie outside the surface $I = I_0$
(b) The surface connects the (unstable) solutions
(c) $I < I_0$, the surface ceases to exist.

Fig. 16. Poincaré sections obtained for the perturbed saddle connection. All Portraits are structurally stable.

Fig. 17. Nonintersecting invariant manifolds in the (ϕ,v,t)-space.

Fig. 18. Poincaré section for intersecting manifolds. P_1 is the forward iteration of P_0, P_{-1} and P_{-2} are the backward iterations of P_0.

Fig. 19. Example of intersecting manifolds in the (ϕ,v,t)-space. The inlet shows the relevant part of Poincaré section.

Fig. 20. Erratic behavior of points lying close to manifold intersection. Domains D_1 and D_2 (respectively D_{-1} and D_{-2}) are the first and second forward (respectively backward) iteration of D_0.

Fig. 21. The values of ε and ω for which the chaotic behavior was observed in the numerical-analog experiments [16].

Fig. A1. An example of possible synchronization zones. Note that the zones for "large" M and N are narrow, and these for small ω are low.

Fig. B1. Examples of a heteroclinic and a homoclinic structure. (a) and (b) show a heteroclinic and a homoclinic orbit of an autonomous system. (c) and (d) show structures which may be obtained when a small perturbation is applied.

Fig. B2. The stable and unstable manifolds and solutions on them taken for the Poincaré section at $t = t_0$.

Fig. B3. The saddle connection Γ_0 for the pendulum with constant forcing.

Fig. B4. A Poincare section of (B9) obtained for $\left|\frac{a}{b}\right| > \left|\frac{B}{A}\right|$.

Fig. B5. The (a,b)-parameter plane. W^u and W^s intersect transversally iff a and b lie within shaded regions. Note that the picture is valid only for small ε and that slope of the regions boundaries at the origin is equal to $\pm B/A$.

References

[1] M. Odyniec, L.O. Chua, "Josephson Junction Circuit Analysis via Integral Manifolds," IEEE Trans. Circuits and Systems, Vol. CAS-30, May 1983.

[2] B.D. Josephson, "Supercurrents Through Barriers," Advan. Phys. Vol. 14 (1965) pp. 419-451.

[3] H. Lübbig, "Progress in Physics of Josephson Junctions," SQUID'80, Berlin, New York, 1980.

[4] E.A. Barbashin and V.A. Tabueva, "Dynamical Systems with a Cylindrical Phase Space" Moscow, 1969 (in Russian).

[5] Ya. S. Baris, V.I. Fodchuk, "Bounded Solutions in Nonlinear Singularly Perturbed Systems via Integral Manifolds," Ukr. Math. Journal, Vol. 22, No. 1, pp. 3-11, 1970 (in Russian).

[6] N.N. Bogoliubov and Y.A. Mitropolskii, Asymptotic Methods in the Theory of Nonlinear Oscillations, Gordon and Breach, New York, 1961.

[7] Y.A. Mitropolskii and O.B. Lykova, Integral Manifolds in Nonlinear Mechanics, Nauka, Moscow, 1973 (in Russian).

[8] J.K. Hale, Ordinary Differential Equations, R. Krieger, New York, 1980.

[9] V.A. Pliss, Nonlocal Problems of the Theory of Oscillations, Academic Press, New York, 1966.

[10] S. Smale, "Differentiable Dynamical Systems," Bull. Amer, Math. Soc. 73 (1967), pp. 747-817.

[11] M.C. Irwin, "Smooth Dynamical Systems", London 1978.

[12] J. Guckenheimer and P.J. Holmes, Nonlinear Oscillations, Dynamical Systems and Bifurcation of Vector Fields, Springer, 1983.

[13] B.D. Greenspan and P.J. Holmes, "Homoclinic Orbits, Subharmonics and Global Bifurcation in Forced Oscillations," in Nonlinear Dynamics and Turbulence, ed. G. Barenblatt, Pitman 1983.

[14] V.K. Melnikov, "On the Stability of the Center for Time-Periodic Perturbations," Trans. Moscow Math. Soc. 12(1963) pp. 1-57.

[15] E. Ben-Jacobi, I. Goldhirsch, Y. Imry, and S. Fishman, "Intermittent Chaos in Josephson Junctions," Phys. Rev. Letters 49 (1982) pp. 1599-1602.

[16] B.A. Huberman, J.P. Crutchfield and N.H. Packard, "Noise Phenomenon in Josephson Junctions," Appl. Phys. Lett. 37 (1980) pp. 750-752.

[17] R.Y. Chiao et al, "Phase Instability Noise in Josephson Junctions," AIP Conf. Proc. 44 (1978) pp. 259-263.

[18] L.N. Belyustina and V.N. Belykh, "The Global Subdivision of Cylindrical Phase Space of a Nonautonomous System," Diff. Uravneniya 9(1973), pp. 595-608.

[19] V.N. Belykh, N.F. Pederson, O.H. Soerensen, "Shunted-Josephson-Junction Model I,II," Phys. Rev. B, Vol. 16, pp. 4753-4871, 1977.

[20] Ch. Hayashi, Nonlinear Oscillations in Physical Systems, McGraw-Hill, New York 1964.

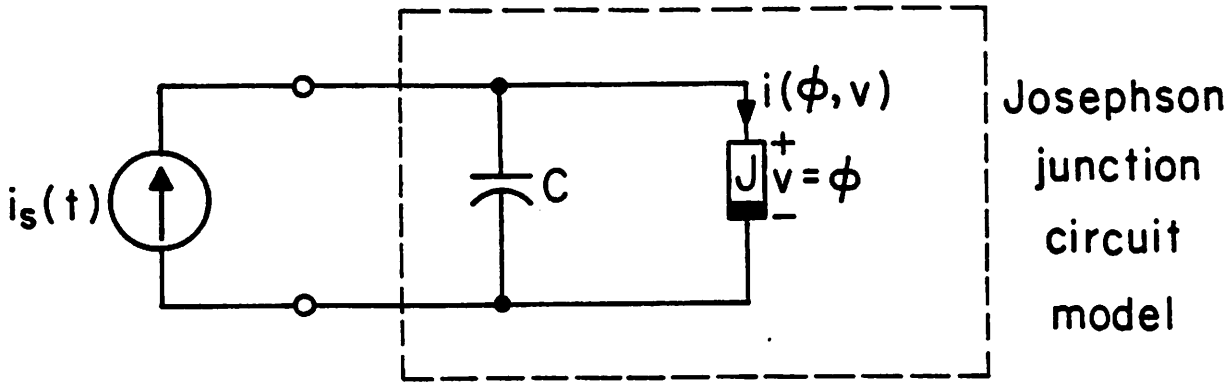

Fig. 1

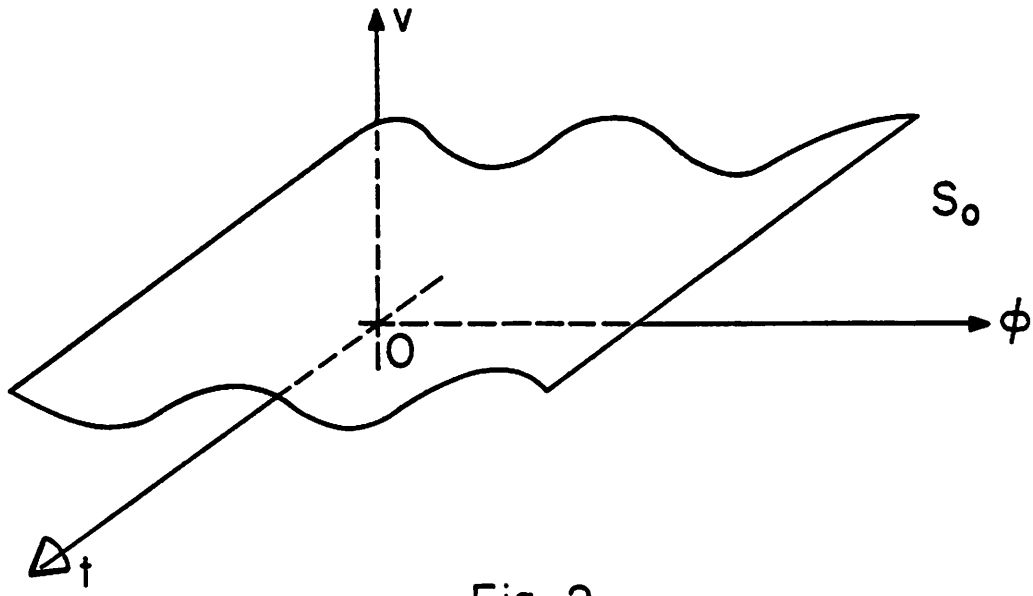

Fig. 2

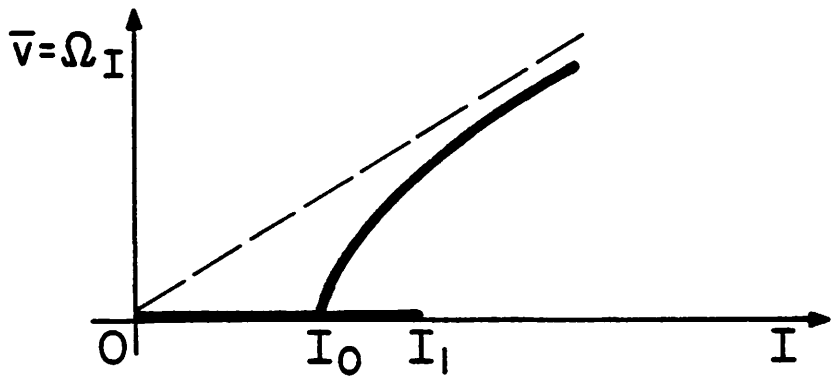

Fig. 3

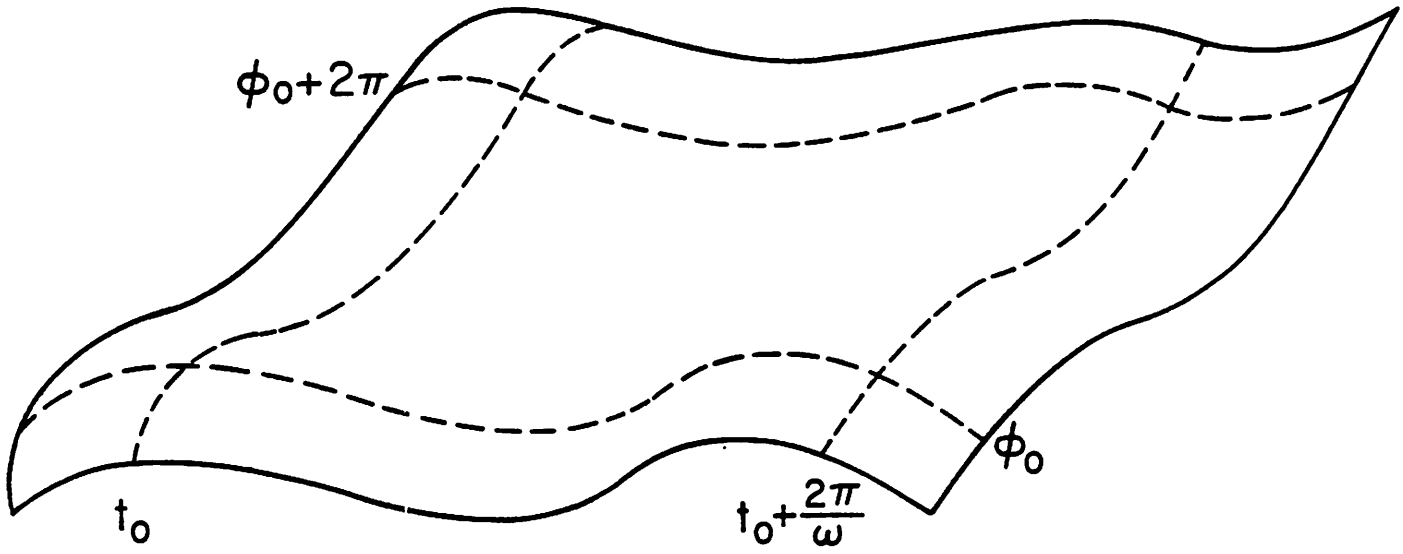
$\phi_0+2\pi$
ϕ_0
t_0
$t_0+\frac{2\pi}{\omega}$

(a)

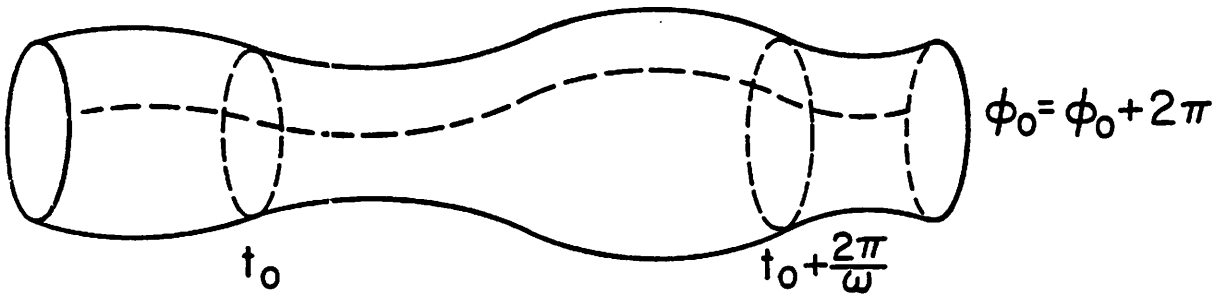
$\phi_0=\phi_0+2\pi$
t_0
$t_0+\frac{2\pi}{\omega}$

(b)

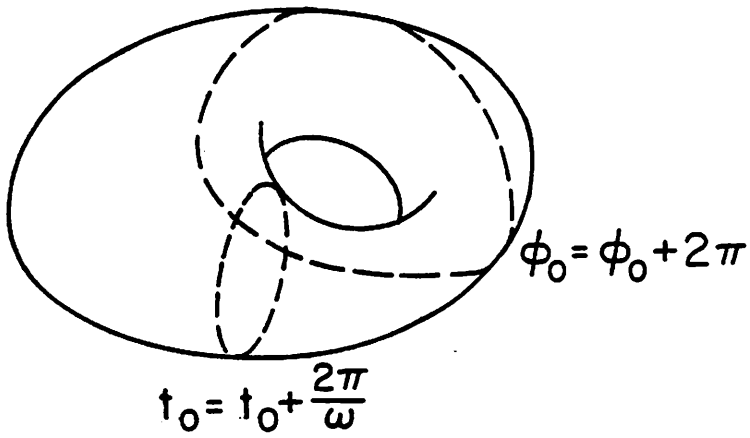
$\phi_0=\phi_0+2\pi$
$t_0=t_0+\frac{2\pi}{\omega}$

(c)

Fig. 4

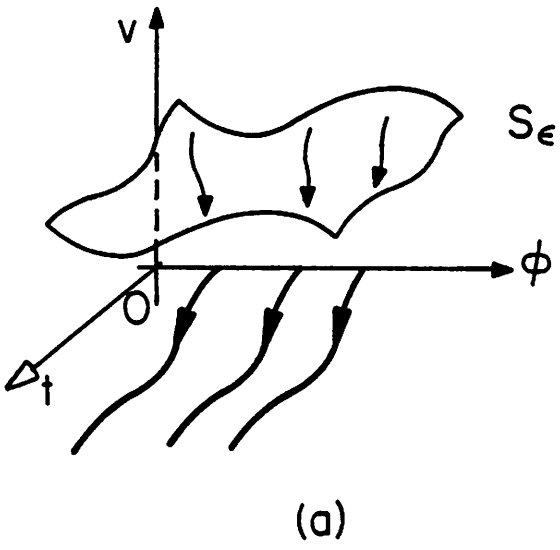

(a)

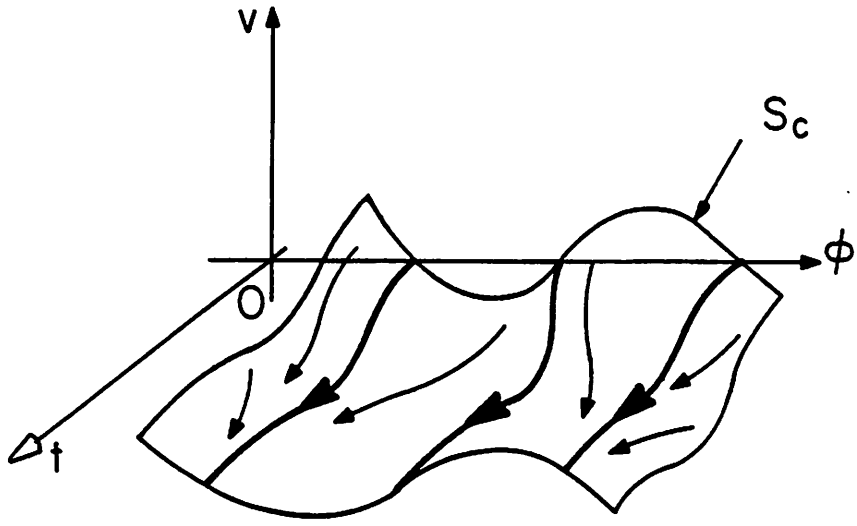

(b)

Fig. 5

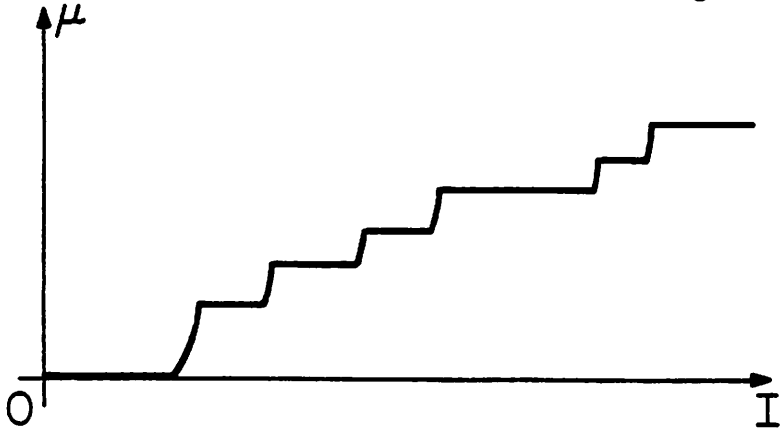

Fig. 6

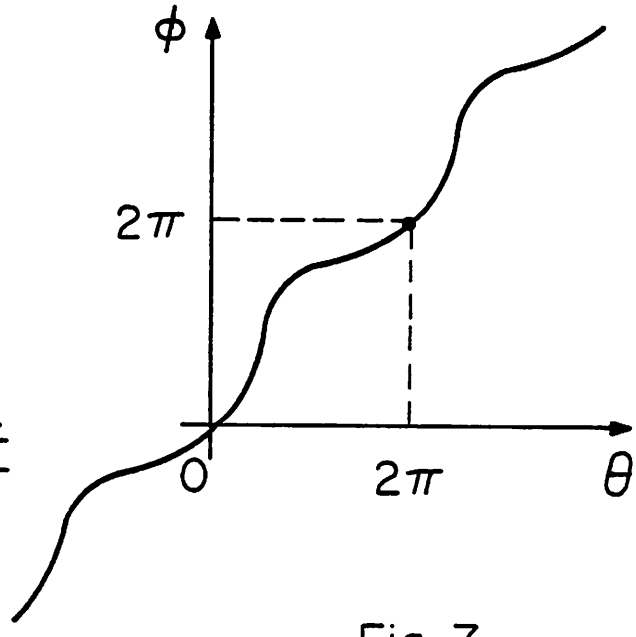

Fig. 7

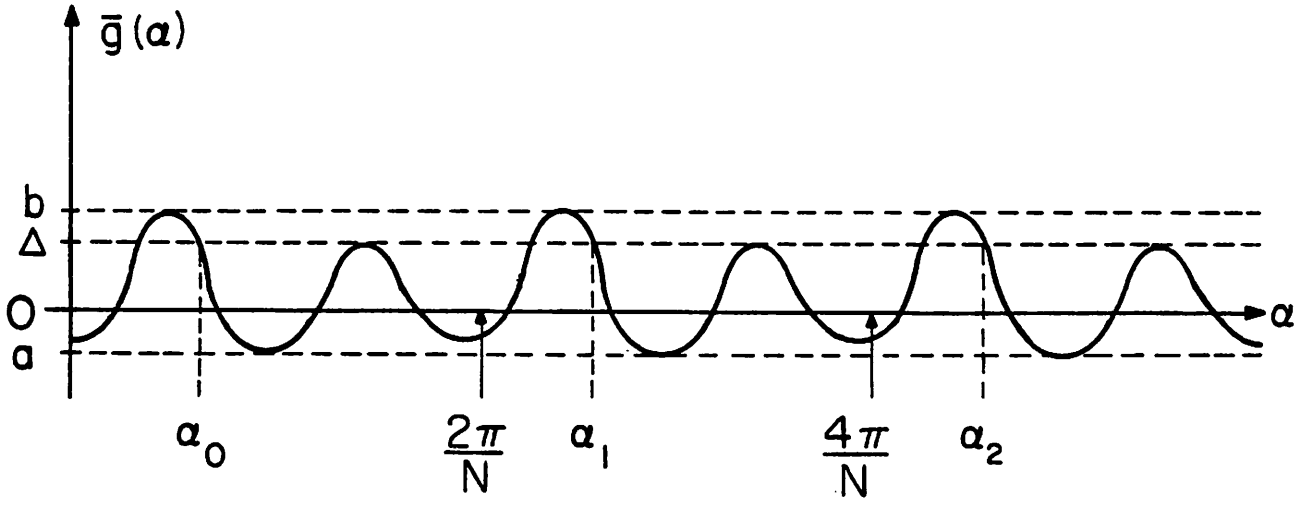

Fig. 8

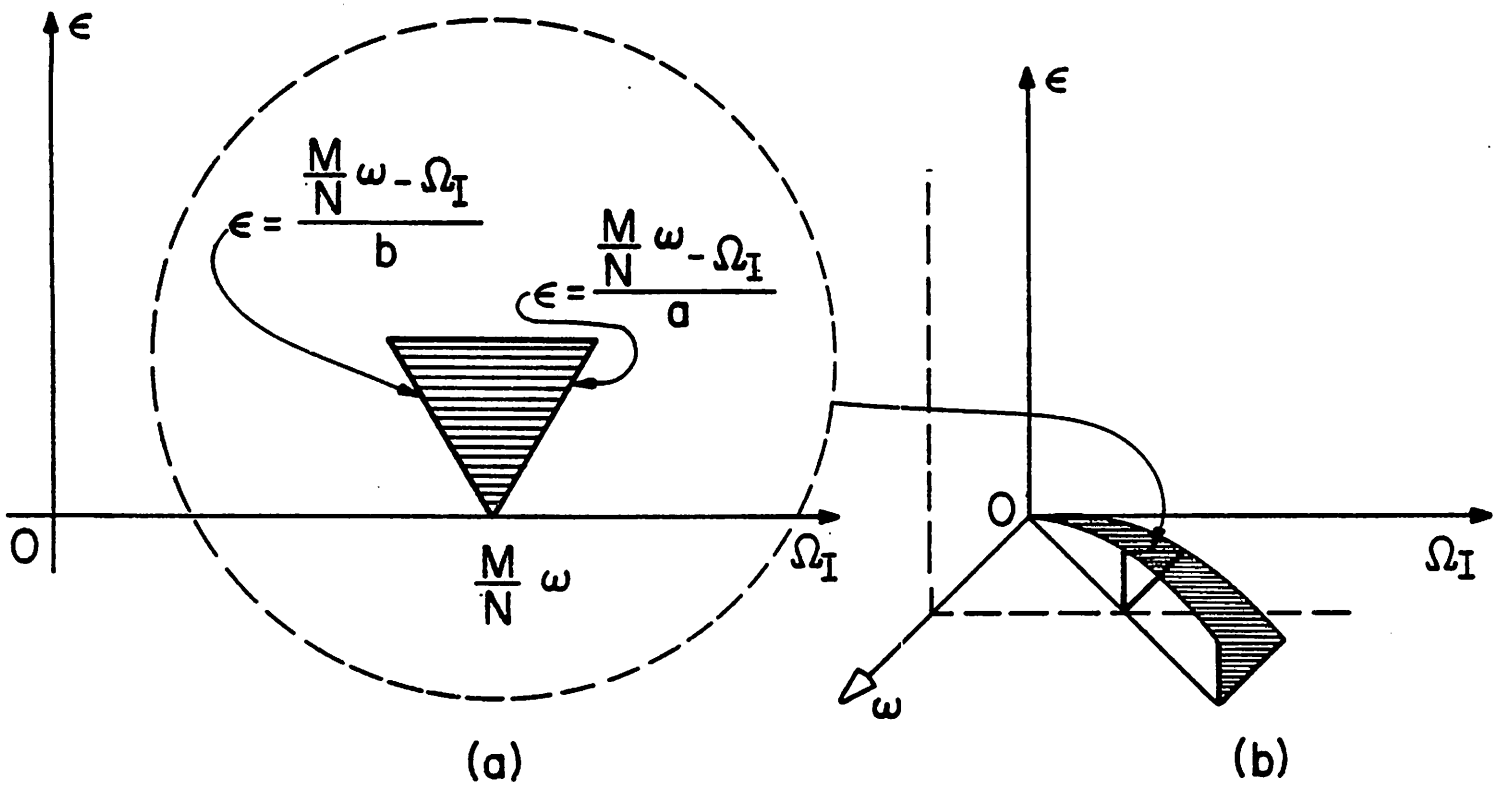
ϵ
$\epsilon = \frac{\frac{M}{N}\omega - \Omega_I}{b}$
$\epsilon = \frac{\frac{M}{N}\omega - \Omega_I}{a}$
0
$\frac{M}{N}\omega$
Ω_I
(a)
ϵ
0
Ω_I
ω
(b)

Fig. 9

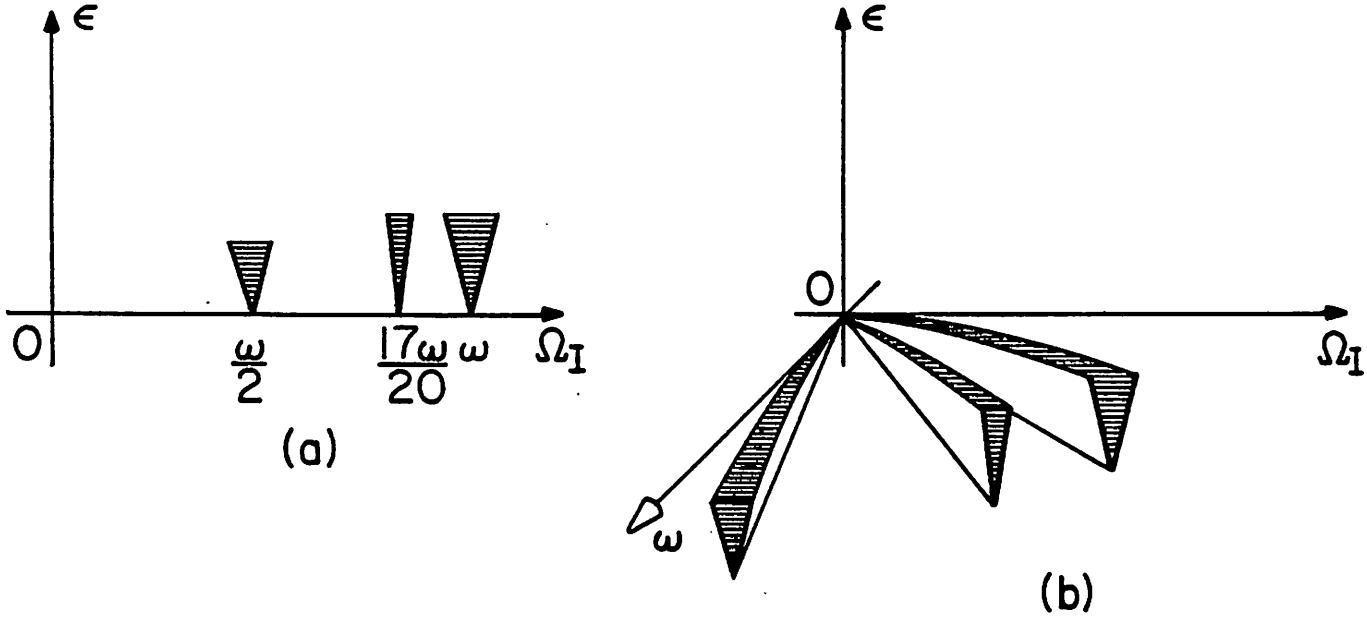
ϵ
0
$\frac{\omega}{2}$
$\frac{17\omega}{20}$
ω
Ω_I
(a)
ϵ
0
Ω_I
ω
(b)

Fig. 10

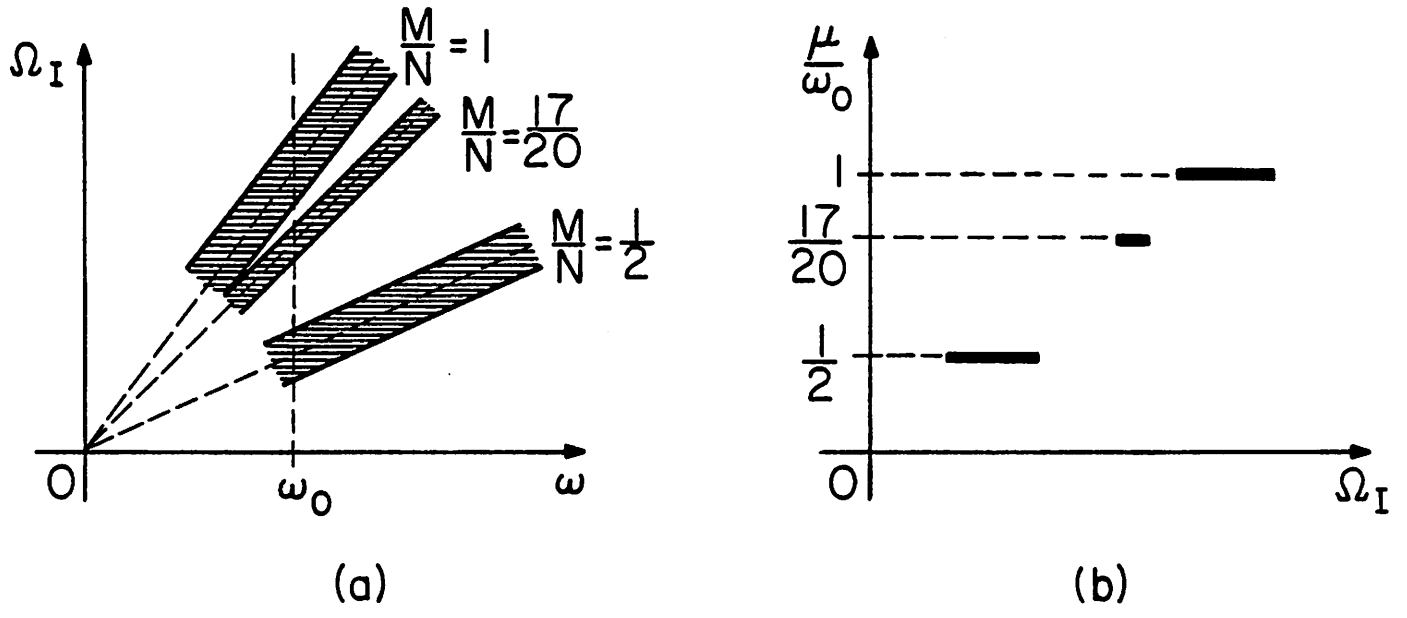
Ω_I
$\frac{M}{N}=1$
$\frac{M}{N}=\frac{17}{20}$
$\frac{M}{N}=\frac{1}{2}$
1
0
ω_0
ω
(a)
$\frac{\mu}{\omega_0}$
1
$\frac{17}{20}$
$\frac{1}{2}$
0
Ω_I
(b)

Fig. 11

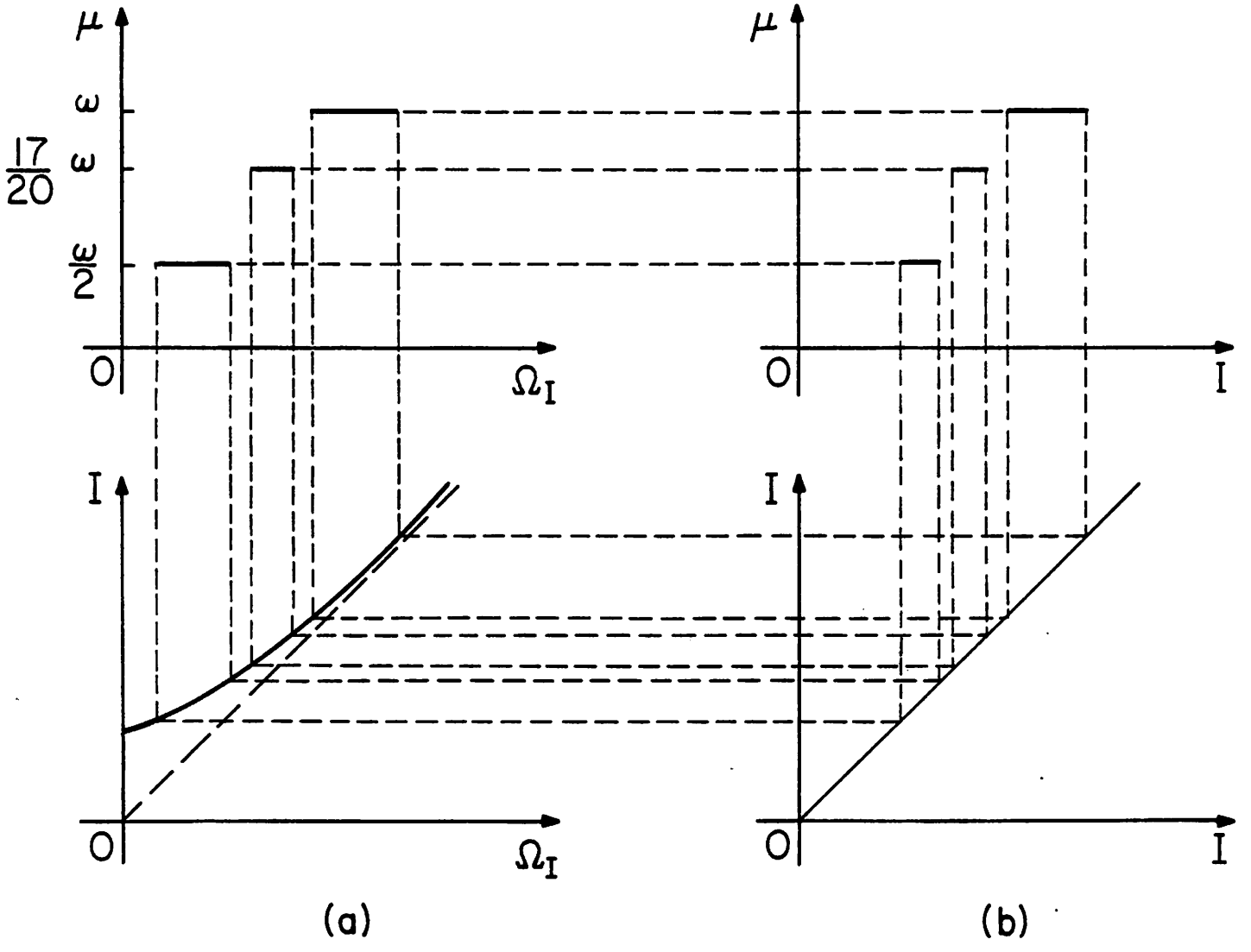
μ
ω
$\frac{17}{20}\omega$
$\frac{\omega}{2}$
0
Ω_I
I
0
Ω_I
(a)
μ
0
I
I
0
I
(b)

Fig. 12

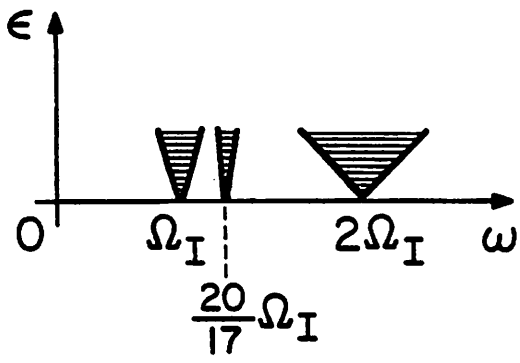

Fig. 13

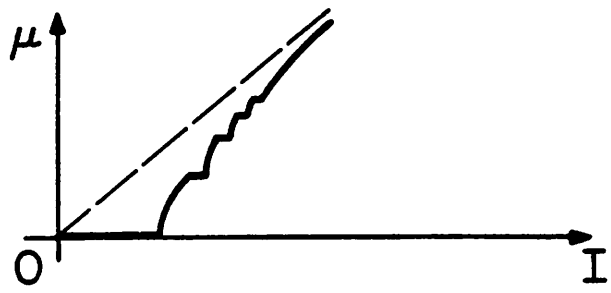

Fig. 14

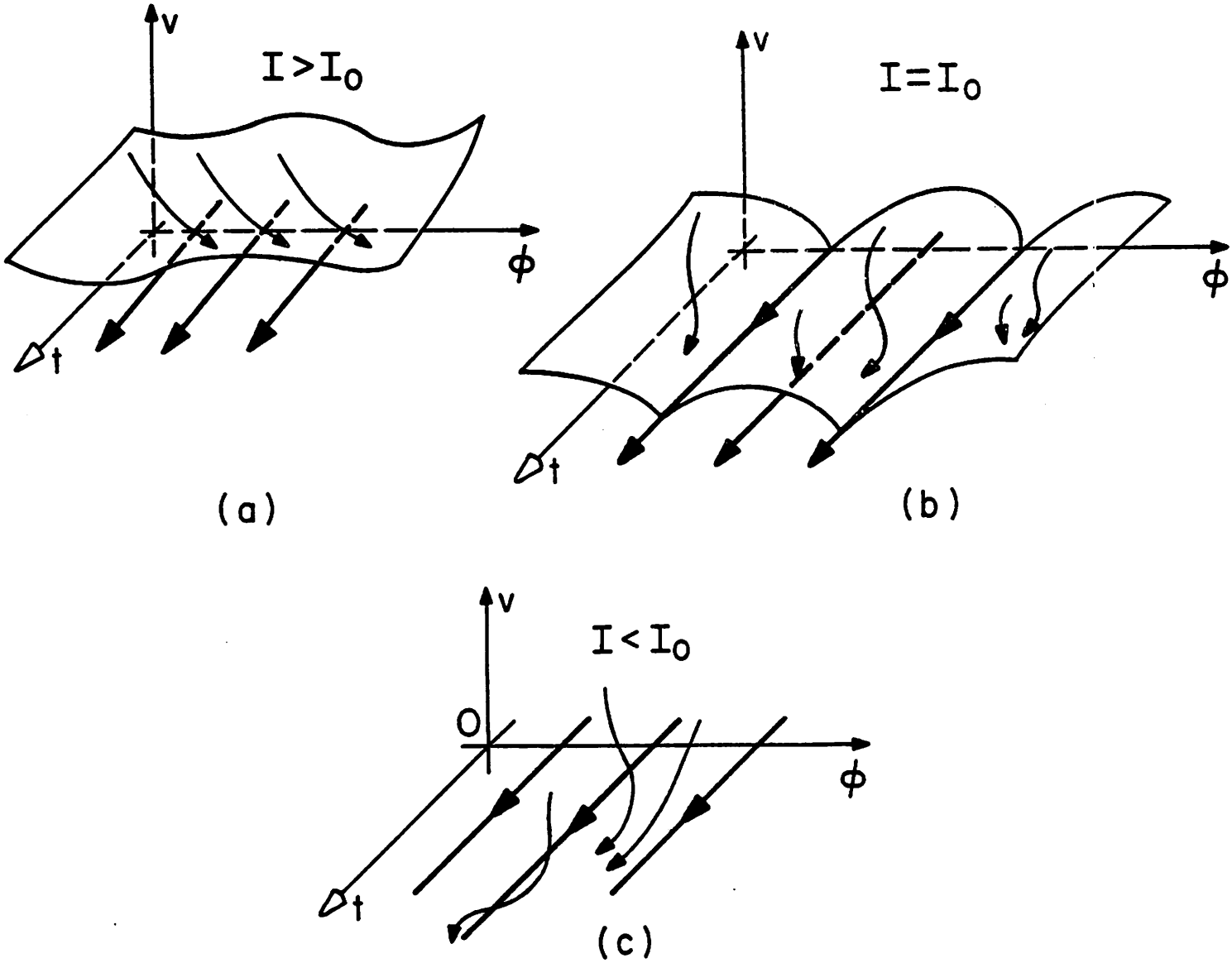

Fig. 15

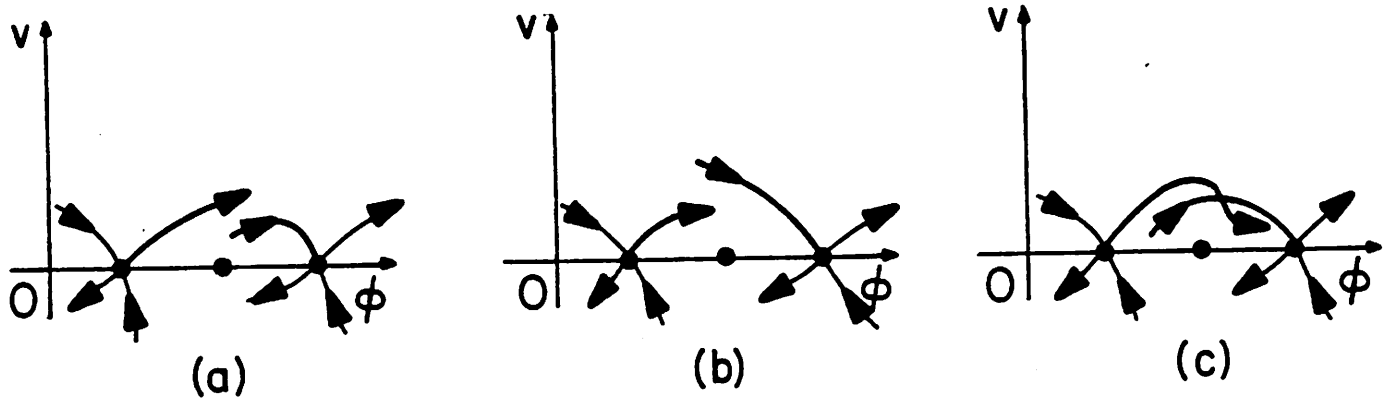

Fig. 16

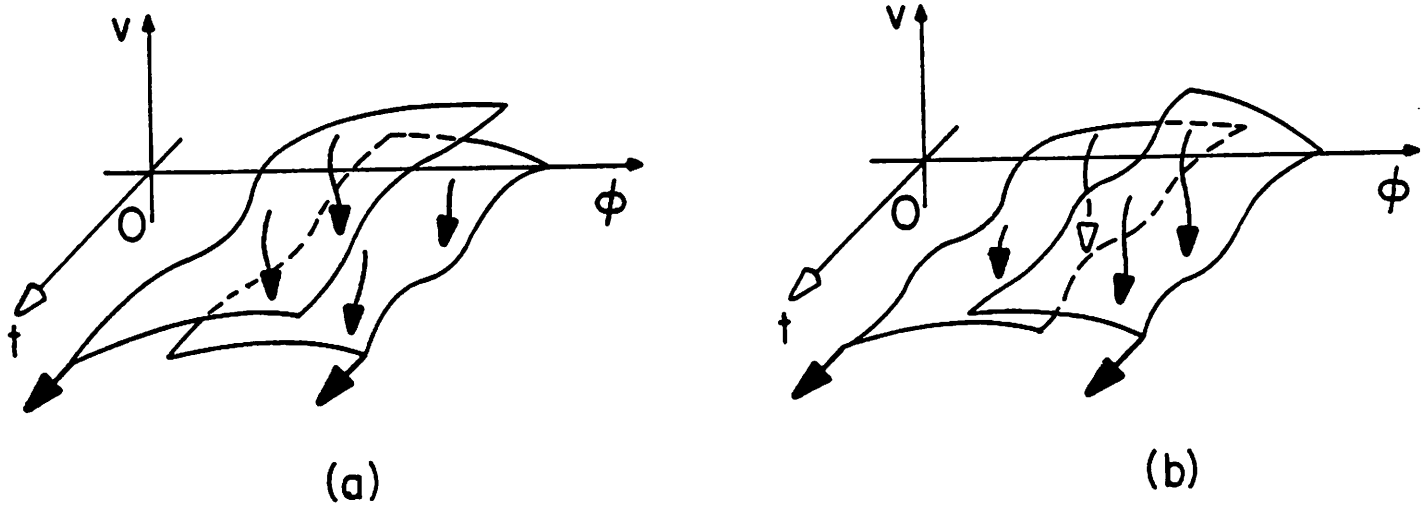

Fig. 17

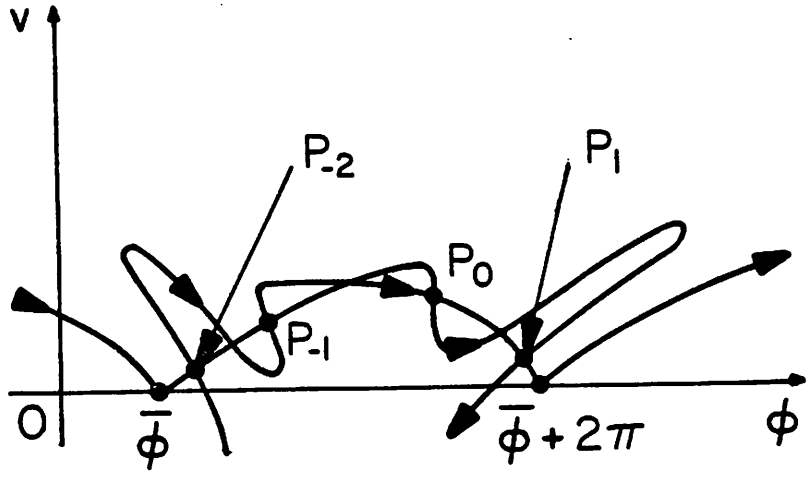

Fig. 18

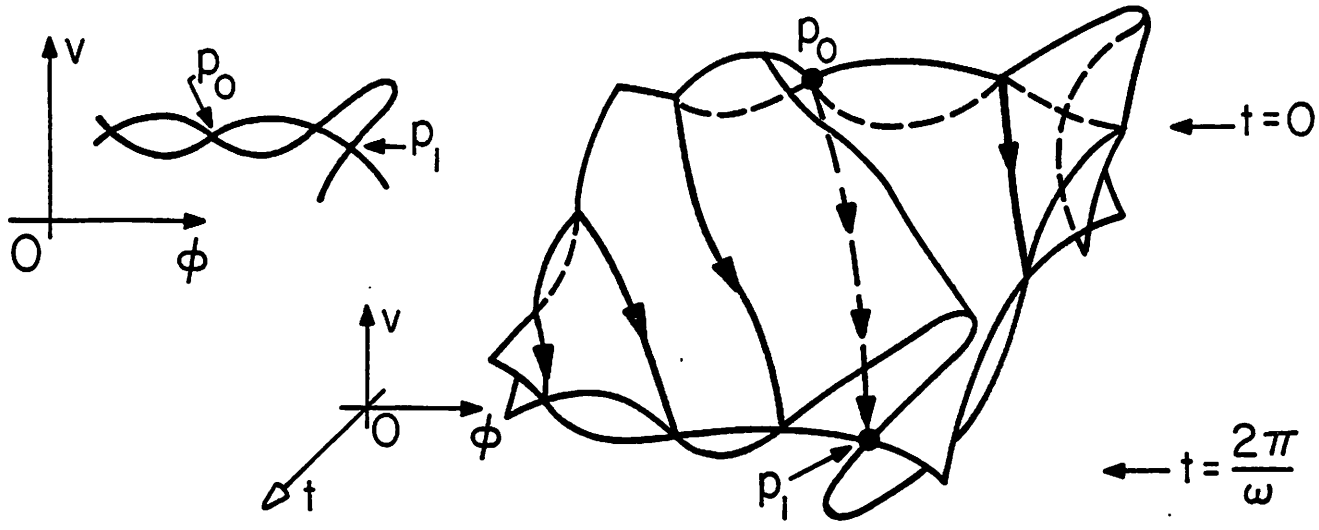

Fig. 19

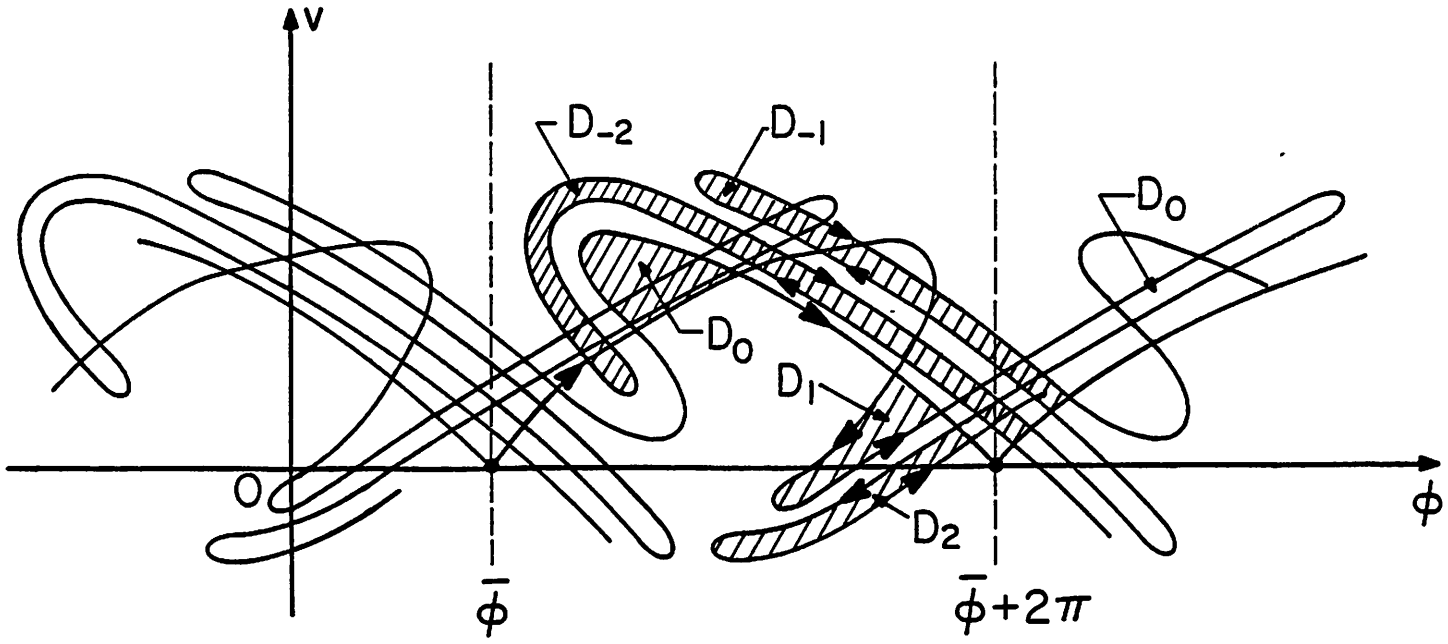

Fig. 20

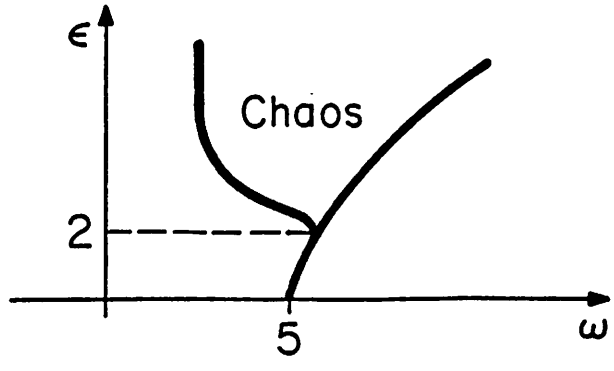

Fig. 21

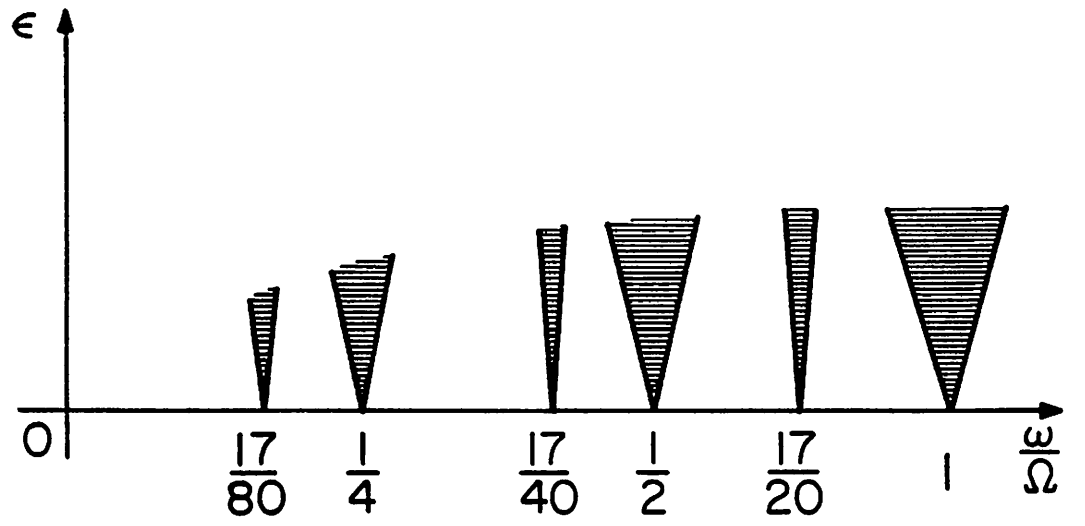

Fig. A1

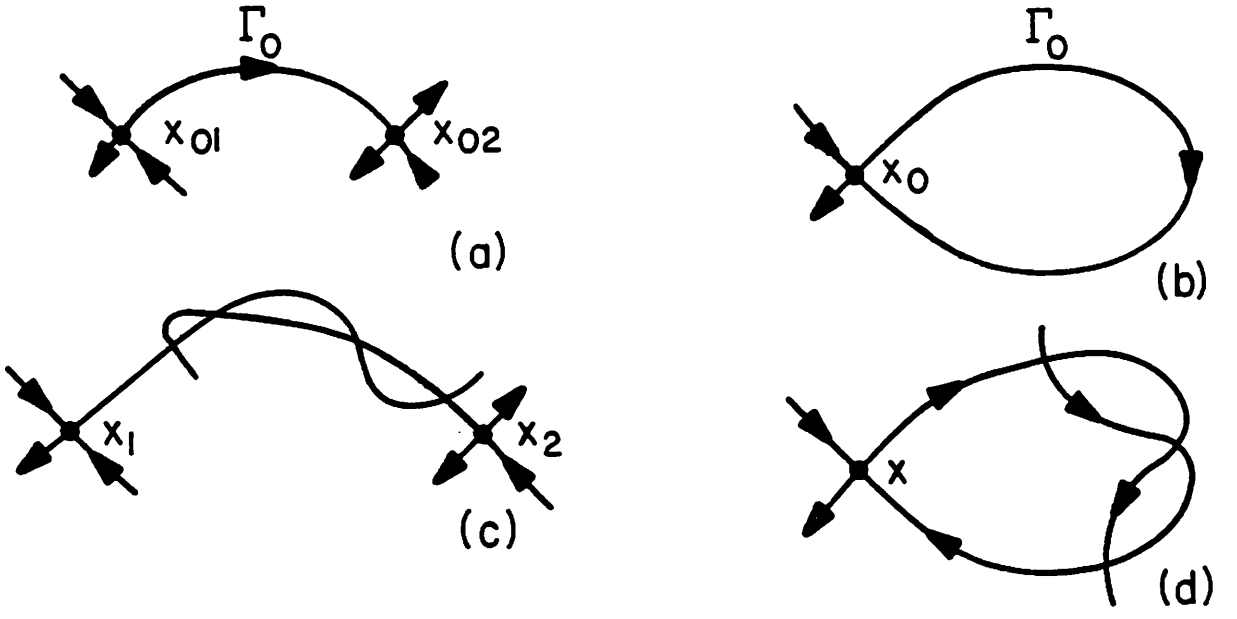

Fig. B1

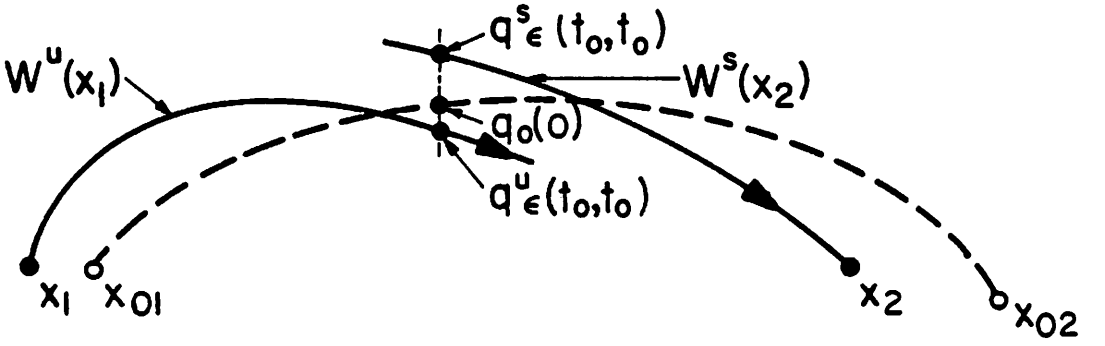

Fig. B2

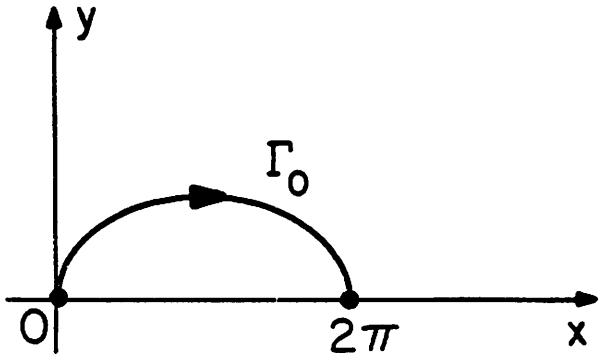

Fig. B3

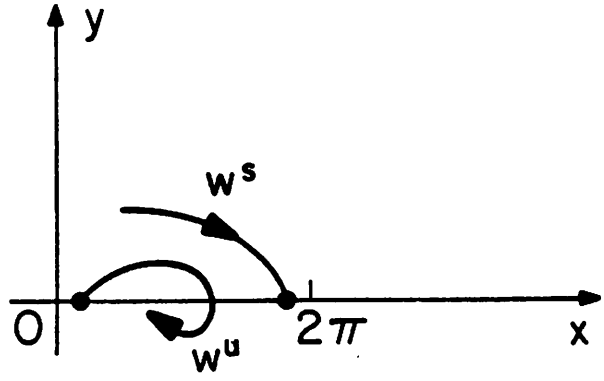

Fig. B4

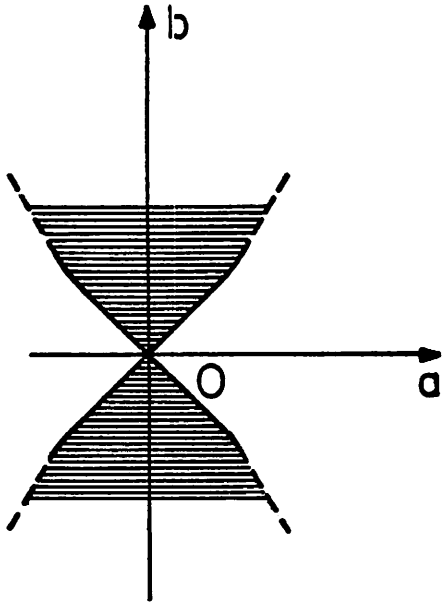

Fig. B5